Chemical Geology 510 (2019) 140–165

Contents lists available at ScienceDirect

Chemical Geology

journal homepage: www.elsevier.com/locate/chemgeo

Invited review article

A continental perspective of the seawater $^{87}Sr/^{86}Sr$ record: A review

Bernhard Peucker-Ehrenbrink[a,*], Gregory J. Fiske[b]

[a] Woods Hole Oceanographic Institution, Woods Hole, MA 02543, USA
[b] Woods Hole Research Center, Falmouth, MA 02540, USA

ARTICLE INFO

Editor: J. Gaillardet

Keywords:
Strontium
Seawater
River
Isotope
Paleoceanography
Bedrock geology

ABSTRACT

Before submarine hydrothermal vents were discovered, the $^{87}Sr/^{86}Sr$ record of seawater was interpreted as a mixture of unradiogenic basaltic and radiogenic granitic continental runoff, strongly buffered by contributions from carbonate weathering. Since the discovery of submarine hydrothermal vents this record has generally been viewed as a mixture of multiple components of which radiogenic continental runoff and unradiogenic submarine hydrothermal fluids are the most significant. A critical review of sources of Sr to seawater indicates that the Sr budget of the modern ocean requires ~1.4×10^{10} mol yr^{-1} of submarine hydrothermal Sr to balance the present-day $^{87}Sr/^{86}Sr$ of freshwater inputs. This flux is about twice what observations of ocean crust alteration and hydrothermal inputs seem to support. The globally averaged, bias-corrected, and Sr flux-weighted $^{87}Sr/^{86}Sr$ of rivers and submarine groundwater discharge is 0.7103–0.7108, and thus significantly less radiogenic than the average $^{87}Sr/^{86}Sr$ of the upper continental crust (> 0.72). Global analyses of runoff from large-scale drainage regions as well as 76 individual river basins with large dissolved Sr fluxes to the ocean reveal positive correlations between the dissolved riverine $^{87}Sr/^{86}Sr$ and the average bedrock age of drainage regions and individual river basins. The current flux of continental Sr to the ocean is biased towards contributions from younger bedrock (331 Myr) compared to the average bedrock age of the exorheic land area (445 Myr). This correlation supports the notion that variations in the marine $^{87}Sr/^{86}Sr$ are influenced by variations in the composition and age structure of exorheic continental bedrock. Quantitative evaluation of the average age of exorheic bedrock, weighted according to the dissolved Sr flux, indicates that the temporal variations of this parameter that are required to account for the observed temporal variations in the $^{87}Sr/^{86}Sr$ of seawater depend primarily on the slope of the correlations between dissolved $^{87}Sr/^{86}Sr$ and bedrock age. The required variations in average exorheic bedrock age are consistent with changes predicted by the paleogeologic reconstructions of the Phanerozoic and appear to be geologically sensible. The data imply that improvements in our understanding of the driving forces of changes in $^{87}Sr/^{86}Sr$ and other radiogenic isotope records of seawater critically depend on improved reconstructions of paleogeology, paleogeography and paleohydrology.

1. Introduction

Strontium plays an outsized role in geochemistry. As a moderately incompatible trace element during melting of the Earth's mantle, it is enriched > 10-fold in the continental crust and by a factor of six in mid-ocean ridge basalts relative to Earth's primitive mantle. Its isotope ^{87}Sr is produced by radioactive β^--decay of ^{87}Rb with a half-life of almost 50 billion years (Steiger and Jäger, 1977; Rotenberg et al., 2012). Rubidium, owing to its highly incompatible behavior during mantle melting, is even more strongly enriched than Sr in the continental crust, but less so in mid-ocean ridge basalts, relative to the primitive mantle (Hofmann, 1988). The resulting time-integrated accumulation of ^{87}Sr in the continental crust has created a large contrast in $^{87}Sr/^{86}Sr$ between the radiogenic continental crust and the unradiogenic depleted mantle. The good solubility and conservative behavior of strontium in natural waters influence the flux balance between sources and sinks that produces an isotopically well mixed seawater reservoir (Faure et al., 1965; Hamilton, 1966; Murthy and Beiser, 1968; Mokadem et al., 2015) with only minor depletions in the surface ocean, a globally averaged concentration of 87.4 μM at 35‰ salinity, and a global inventory of 11.6×10^{16} mol (de Villiers, 1999; Charette and Smith, 1999). The seawater Sr reservoir responds to changes in its mass balance with a characteristic response time of 1–2 million years. The $^{87}Sr/^{86}Sr$ of seawater therefore reflects a globally integrated balance of processes that affect the delivery and removal of strontium. For this reason temporal variations in the $^{87}Sr/^{86}Sr$ of seawater have been the focus of numerous

* Corresponding author.
E-mail address: behrenbrink@whoi.edu (B. Peucker-Ehrenbrink).

https://doi.org/10.1016/j.chemgeo.2019.01.017
Received 19 July 2018; Received in revised form 3 January 2019; Accepted 26 January 2019
Available online 07 February 2019

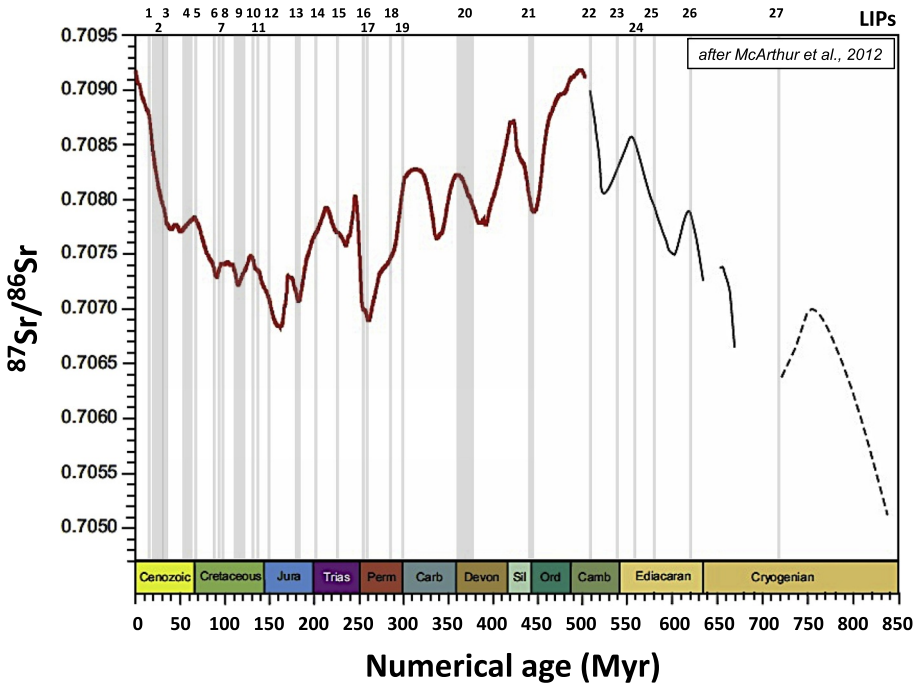

Fig. 1. The record of seawater $^{87}Sr/^{86}Sr$ during the Phanerozoic (red line) and Neoproterozoic (gray line), modified from McArthur et al. (2012). The gray vertical bars indicate the timing of the formation of Large Igneous Provinces after Thorsvik et al. (2008), Jones et al. (2016), Ernst and Youbi (2017): 1 – Columbia River, 2 – Sierra Madre Occidental, 3 – Afar-Arabian, 4 – North Atlantic Igneous Province, 5 – Deccan, 6 – Madagaskar, 7 – Carribean-Colombian & others, 8 – High Arctic-2, 9 – Kerguelen, 10 – Ontong Java & others, 11 – Parana-Etendeka, 12 – Bunbury-Comei, 13 – North Australian Margin, Shatsky Rise & others, 13 – Karoo-Ferrar, 14 – CAMP, 15 – Wrangelia, 16 – Siberian Traps, 17 – Emeishan, 18 – Tarim, Panjal Traps, 19 – Skagerrak, 20 – Kola-Dnieper, Yakutsk-Vilyui, 21 – Suordakh & others, 22 – Kalkarindji, 23 – Wichita, 24 – CIMP pulses, 25 – Franklin & Irkutsk.

studies aimed at extracting from this record information on processes of global importance that affect the mass balance of strontium in seawater.

Over that past six decades the $^{87}Sr/^{86}Sr$ record of seawater has become one of the best-reconstructed marine isotope records with many thousands of high-quality data covering the Phanerozoic and Neoproterozoic (Gast, 1955; Peterman et al., 1970; Veizer and Compston, 1974; Veizer et al., 1999; Shields and Veizer, 2002; for a recent review see McArthur et al., 2012, references therein, and Fig. 1). Temporal variations have been correlated with periods of glaciations (Armstrong, 1971; Palmer and Elderfield, 1985; Blum and Erel, 1995; Vance et al., 2009), mountain building (Raymo et al., 1988; Edmond, 1992; Richter et al., 1992; Krishnaswami et al., 1992), major volcanic eruptions (Kent and Muttoni, 2008) or periods of enhanced submarine hydrothermal activity (Palmer and Elderfield, 1985; Korte et al., 2006), as well as changes in submarine groundwater discharge (termed "runout" by Chaudhuri and Clauer, 1986; Allègre et al., 2010; see also Beck et al., 2013; Trezzi et al., 2016), ocean crust alteration (Spooner, 1976; Davis et al., 2003; Coogan and Dosso, 2015), and total land area (Spooner, 1976). Regionally, variations in climate and sea level can influence the $^{87}Sr/^{86}Sr$ record of marginal seas such as the Mediterranean (Schildgen et al., 2014), and continental freshwater inputs can locally modify the $^{87}Sr/^{86}Sr$ of coastal waters (Ingram and Sloan, 1992; Huang et al., 2011; see also Fig. 8 in Korte et al., 2003).

Despite the impressive seawater record and seven decades of research (e.g. Wickman, 1948; Peterman et al., 1970; Dasch and Biscaye, 1971; Burke et al., 1982; Veizer et al., 1999; McArthur et al., 2012), assessments of the present-day mass balance of strontium in seawater fundamentally disagree. Many studies, represented for instance by Vance et al. (2009) and Pearce et al. (2015), argue that seawater Sr is currently not at steady state. According to this assessment, the flux of radiogenic strontium from the continents is currently elevated because of the unusually large release of radiogenic strontium from recently glaciated terrains that are characterized by large reactive mineral surface areas. According to this view, present continental runoff cannot be a valid proxy for average conditions of the recent past. Significant differences in the stable Sr isotope composition ($^{88}Sr/^{86}Sr$) between sources and sinks of strontium in seawater support this interpretation (Krabbenhöft et al., 2010; Pearce et al., 2015).

The non-steady-state view has been challenged by Allègre et al. (2010), who argue that most previous estimates of continental Sr flux and $^{87}Sr/^{86}Sr$ to seawater are biased, because they do not properly take into account the flux of unradiogenic Sr from ocean islands and island arcs, and in particular neglected continental Sr entering the ocean below sea-level. According to Allègre et al. (2010) the properly weighted global flux of Sr from the continents to seawater has an isotope composition of 0.7101 and represents a longer-term (Pleistocene) global average. This $^{87}Sr/^{86}Sr$ value represents the combined contributions from "continental rivers" ($44 \pm 15\ ng\ g^{-1}$ Sr, 0.7136), surface runoff from island arcs and ocean islands ($35 \pm 10\ ng\ g^{-1}$ Sr, 0.7035) that are significantly less radiogenic than average "continental rivers", as well as unradiogenic submarine Sr from island arcs and ocean islands ($450 \pm 150\ ng\ g^{-1}$ Sr, 0.7035). Together, these continental contributions balance marine contributions to the marine Sr isotope budget. According to this interpretation of the data, present-day conditions do serve as a proxy for the recent past. Interestingly and coincidentally, these continental $^{87}Sr/^{86}Sr$ estimate and steady-state conclusion are identical to those Goldstein and Jacobsen (1987) reached based on data for 23% of the riverine flux (without data for the radiogenic Ganges and Brahmaputra rivers) and without considering continental Sr entering the ocean below sea level. However, we note that the proportions of volcanic rock surface area on "ocean islands" such as Papua New Guinea (35%), Japan (60%), Philippines (70%) and Taiwan (60%) as estimated by Allègre et al. (2010) far exceed proportions determined using digital geologic maps (9.1%, 28%, 14% and 0.7%, respectively, Peucker-Ehrenbrink and Miller, 2004). This, and the assumption that runoff from such rocks has a $^{87}Sr/^{86}Sr$ of 0.7035, results in a very unradiogenic flux from these land areas and help balance the Sr budget of seawater.

The disagreement between interpretations of essentially the same data arises from the uncertainties associated with the fluxes and isotopic compositions of strontium in rivers and submarine discharge of continental groundwaters. Here, we first review the sources of the disagreement with a focus on the continental flux of Sr to seawater, because "river inputs appear to dominate the Nd and Sr isotopic signature of the modern ocean" (Goldstein and Jacobsen, 1987, p. 270). We extend earlier attempts to use spatial geologic data to scrutinize riverine $^{87}Sr/^{86}Sr$ data for spatial biases (Wadleigh et al., 1985; Veizer, 1989; Palmer and Edmond, 1989; Peucker-Ehrenbrink et al., 2010;

Bataille et al., 2014) by employing geographic information systems (GIS, ArcGIS) and digital geologic maps of various spatial and temporal resolution. We argue that such biases exist and attempt to correct for them given our current understanding of the global distributions of bedrock geology and discharge. We then use global correlations to argue that the temporal variations in the $^{87}Sr/^{86}Sr$ of seawater is not primarily caused by variations in the balance between radiogenic continental and unradiogenic submarine hydrothermal sources of Sr to the oceans. Instead we argue that temporal variations primarily reflect the changing composition of continental runoff that is determined by the changing spatial distributions of continental bedrock, climate and drainage patterns through geologic time (e.g. Brass, 1976; Palmer and Elderfield, 1985; Kump, 1989; Peucker-Ehrenbrink et al., 2010). We conclude this review with a quantitative assessment of a parameter that captures the essential variables at the scale of individual river basins and large-scale drainage regions: the Sr-flux-weighted average bedrock age of the exorheic portion of the land surface (T_{bexSr}). Sparse $^{143}Nd/^{144}Nd$ data for globally integrated seawater through the Phanerozoic, $^{143}Nd/^{144}Nd$ data for continental erosion products, and reconstructions of Phanerozoic paleogeology support this interpretation of temporal variations in the $^{87}Sr/^{86}Sr$ of seawater.

Our perspective of the seawater $^{87}Sr/^{86}Sr$ record resembles models proposed before submarine hydrothermal sources of unradiogenic Sr were discovered in 1977 (Corliss et al., 1979). Before this discovery, temporal variations in the marine Sr isotope record were thought to be caused by the changing balance between inputs from young, mantle-derived rocks exposed on the continents that constitute the unradiogenic source, and old continental rocks that release radiogenic strontium, buffered by the weathering of carbonate rocks with an isotope composition similar to seawater (Faure et al., 1965; Veizer and Compston, 1974; Brass, 1976). Initially, the recognition that the $^{87}Sr/^{86}Sr$ of submarine basalts can be altered by interaction with more radiogenic seawater did not mean that this alteration was viewed as an exchange process that could also significantly alter the $^{87}Sr/^{86}Sr$ of seawater (Dasch et al., 1973). However, since the discovery of submarine hydrothermal sources the marine Sr isotope budget has generally, but not exclusively (Palmer and Elderfield, 1985; Kump, 1989), been interpreted as a multi-component mixture of unradiogenic submarine hydrothermal vents near ocean ridges and radiogenic continental sources, with some models making allowance for additional minor end-members as well as temporarily variable compositions and fluxes of end-members (e.g. Albarède et al., 1980, 1981; Goldstein and Jacobsen, 1987; Veizer, 1989; Palmer and Edmond, 1989, 1992; Hodell et al., 1990; Blum and Erel, 1995; Farrell et al., 1995; Butterfield et al., 2001; Davis et al., 2003; Vance et al., 2009). Given our understanding of the importance of submarine hydrothermal circulation, the perspective presented here may appear counterintuitive. We therefore emphasize that our perspective does not negate that hydrothermal Sr fluxes to seawater have varied in the geologic past. In fact, some variations in the $^{87}Sr/^{86}Sr$ of seawater appear to coincide with changes in ocean spreading rate (Fig. 2), a common but imperfect measure of chemical fluxes from the oceanic crust into seawater. However, our current inability to independently quantify submarine hydrothermal fluxes of strontium through time compels us to emphasize a terrestrial end-member model that will need to be adjusted once submarine hydrothermal Sr fluxes can be properly and independently quantified.

2. Quantitative bedrock geology of watersheds

2.1. Methods to quantify bedrock geology

It has long been recognized that the geologic composition and bedrock age of watersheds strongly influence the inorganic composition of rivers and streams. Reeder et al. (1972) found that three factors that are related to bedrock mineralogy explain > 95% of the variance of the dissolved chemical composition of the Mackenzie River and its tributaries. Meybeck (1986, 2005) of small watersheds with uniform geology confirm what Reeder et al. (1972) found in a large drainage basin, and led to the definition of endmember chemical compositions of natural waters. Goldstein and Jacobsen (1987, p. 246) conclude that the "isotopic composition of Nd and Sr in a river may be controlled primarily by the average age of the rocks in its drainage basin."

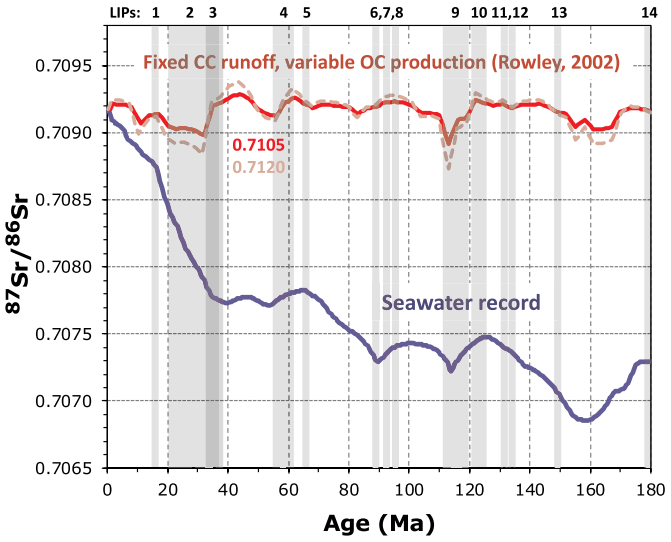

Fig. 2. The $^{87}Sr/^{86}Sr$ record of seawater of the past 180 Myr (solid blue line) compared to two estimated seawater $^{87}Sr/^{86}Sr$ (red and pink lines) records that assume constant continental, but variable hydrothermal Sr fluxes. Variations in the hydrothermal input have been parameterized assuming the Sr flux is linearly correlated with ocean crust production (Rowley, 2002). The continental flux was held constant at the modern value, whereas average $^{87}Sr/^{86}Sr$ of continental runoff was assumed to be the best current estimate (0.7105, solid red line) or slightly more radiogenic (0.7120, pink line). Note the inflection to less radiogenic values in both records at ~55–60 Ma, ~112 Ma, and ~155–170 Ma. Gray vertical bars indicate emplacement of LIPs (same identifiers as in Fig. 1).

The earliest quantitative methods employed to investigate the lithologic composition of drainage basins involved planimetric measurements of topographic and geologic maps (Reeder et al., 1972). These agree very well with modern data (Table 3 in Peucker-Ehrenbrink et al., 2010). Modern data analysis use geographic information systems (GIS) and digital geologic maps (e.g. Peucker-Ehrenbrink and Miller, 2002, 2003, 2004, 2007a, 2007b; Peucker-Ehrenbrink, 2009; Peucker-Ehrenbrink et al., 2010; Bataille and Bowen, 2012; Bataille et al., 2014), the same approach used in this review.

2.2. New data for exorheic watersheds

Average bedrock ages of individual watersheds range span more than two orders of magnitude from as young as 22 Myr (Fly River, Papua New Guinea) to as old as 2524 Myr (Cauvery River, India). "Bedrock ages" refer to depositional ages of sedimentary rocks, eruption ages of volcanic rocks, high-temperature cooling ages of intrusive rocks, and at least medium-grade metamorphic conditions for metamorphic rocks. Sedimentary rocks include siliciclastic and carbonate lithologies, but do not quantify the proportion of the latter that strongly affects dissolved Sr in rivers. We also emphasize that depositional ages of siliciclastic rocks are generally much younger than model ages that reflect the crustal residence times of their precursors. Table 1 summarizes important statistical measures of the bedrock analysis. For watersheds with old average bedrock ages the issue of overestimating ages by using rectangular age distributions for individual bedrock units has to be addressed, as the extent of bias depends on the resolution of the geologic bedrock maps used. Coarse-scale maps with few

Table 1
(S1): River basin bedrock ages (with 1.s.d. uncertainties, and half-range uncertainties that are more conservative in cases where age distributions deviate substantially from normal [see Fisher's kurtosis and skewness]), lithologic compositions (in km^2 and % of area) for the entire (left side) and the sampled portion (right side) of the respective river drainage basin. Lithological composition has been grouped in three main categories: sedimentary bedrock, volcanic bedrock, and endogenous (igneous and metamorphic) bedrock. Endogenous bedrock values in italics assume that "Precambrian (undifferentiated)" polygons reflect endogenous bedrock. Area covered by water, ice, ocean crust, undated lithologies or undifferentiated bedrock is listed as "Other" (in km^2 and % of area). Sample locations for the "Sampled Drainage Basin" parameters refer to locations used to sample rivers for strontium concentration and isotope analyses in the original references (Peucker-Ehrenbrink, 2018). If multiple estimates are provided for a single river, different bedrock maps have been used for the analyses. For instance, "_USGS" after the river name denotes the use of a global bedrock map, whereas "_HR" refers to regional maps (North American, South America, SE Asia, Europe) of higher spatial resolution. An asterisk following a river name refers to analysis done using bedrock maps of Alaska, Canada and the conterminous US following methods of Peucker-Ehrenbrink and Miller (2002, 2003, 2004, 2007a/b) and Peucker-Ehrenbrink et al. (2010). Gray highlights for different river basins are for better visibility.

#	River basin	Entire Drainage Basin							Sediments	Volcanics
		Size_all	Size_dated	Av. Age	±S.D.	Range/2	Fisher's			
	$n = 76$	km^2	km^2	Myr	Myr	Myr	Skewness	Kurtosis	km^2	km^2
1	Amazon_USGS	6,030,187	6,028,209	777	162	418	−0.06683	−0.63136	4,111,716	69,072
	Amazon_HR	6,030,070		678	158	306	−0.04006	−1.18227	4,224,639	377,659
2	Congo	3,704,611		1064	189	451	−0.05624	−0.64731	2,362,204	6317
3	Ob	3,510,698	3,495,769	231	34	79	−0.07327	−0.85390	3,298,257	41,086
4	Mississippi*	3,204,093		309	7				3,028,422	49,802
5	Nile	2,996,828		871	179	441	−0.08290	−0.42185	1,516,773	183,158
6	Parana	2,625,803		370	92	195	−0.01829	−0.89505	1,940,517	337,546
	Parana_USGS	2,625,763	2,625,763	372	41	125	−0.03165	−0.27673	1,966,014	325,358
7	Lena	2,350,906	2,338,045	816	90	206	−0.02296	−0.71314	1,671,969	101,183
8	Yenisey	2,300,368	2,285,368	543	74	161	−0.02813	−0.92317	1,432,425	594,243
9	Yangtze_USGS	1,909,321	1,888,283	393	62	124	−0.01702	−1.08116		
	Yangtze	1,909,306		418	59	141	−0.01387	−0.85433	1,721,329	61,647
10	Niger	1,838,748	1,833,361	1016	220	490	−0.06517	−0.82793	1,069,319	23,745
11	Mackenzie*	1,716,243		693	18				1,455,608	27,183
12	Zambezi	1,378,106		963	224	438	0.00137	−1.17494	655,357	26,180
13	Nelson*	1,097,716		766	12				866,995	44,730
14	Ganges	958,389	954,411	737	177	344	0.04646	−1.13002	652,608	89,163
	Ganges_USGS	953,422	944,109	776	340	563	−0.02741	−1.15562		
15	Orinoco	938,396		697	163	327	−0.01795	−1.07747	642,491	52,148
	Orinoco_USGS	938,395	938,395	835	243	503	−0.03486	−1.10245	552,722	2109
16	Indus	854,666	829,664	398	104	209	0.12070	−1.01577	583,207	26,284
	Indus_USGS	849,761	843,922	313	81	158	−0.06943	−1.16583		
17	Yukon*	852,389		280	12				565,906	117,621
18	Mekong_USGS	796,433	742,832	244	20	52	−0.13179	−0.42424		
	Mekong	774,275		215	21	58	−0.09910	−0.28988	695,048	17,680
19	Danube_HR	786,808		262	29	75	−0.02351	−0.49681	663,786	20,285
	Danube	786,806		253	56	137	0.09559	−0.64980	659,882	27,339
	Danube_HR	163,007		200	24	63	−0.08034	−0.56841	151,053	2738
20	Murray-Darling_USGS	775,198	773,423	149	5	16	0.14049	−0.20091		
	Murray-Darling	775,198		191	16	41	−0.01404	−0.31900	686,374	29,281
21	Tocantins	772,469		1173	227	553	−0.11469	−0.67483	410,553	2822
	Tocantins_USGS	772,408		1123	249	587	0.11535	−0.73700	417,152	9135
22	Huang He_USGS	761,253	761,030	279	30	66	0.03188	−1.02177		
	Huang He	761,224		366	51	103	0.01929	−1.03431	700,905	0
23	Columbia	715,064	699,827	258	7	21	0.15381	−0.02945		
24	Brahmaputra_-USGS	698,074	599,022	406	100	201	0.02801	−1.13406		
	Brahmaputra	626,185		524	151	285	−0.04326	−1.09427	408,420	13,842

(*continued on next page*)

Table 1 (*continued*)

#	River basin	Entire Drainage Basin							Sediments	Volcanics
		Size_all	Size_dated	Av. Age	±S.D.	Range/2	Fisher's			
	$n = 76$	km^2	km^2	Myr	Myr	Myr	Skewness	Kurtosis	km^2	km^2
25	Irrawaddy_USGS	656,379	374,700	499	135	299	−0.09823	−0.71564		
26	Kolyma	652,842		292	30	76	−0.00160	−0.44259	533,891	84,798
27	Orange	556,637	556,384	886	167	382	0.04265	−0.93434	431,723	74,869
28	Dnieper	509,808		374	39	97	−0.08954	−0.57133	453,453	0
29	N. Dvina	440,174	438,357	310	32	72	−0.01376	−0.84796	438,357	
30	Indigirka	440,114	439,333	163	16	39	−0.06745	−0.68471	405,230	14,322
31	Don	437,300		98	18	45	−0.07116	−0.51609	434,236	0
32	Colorado	436,859	436,859	209	6	16	−0.08723	−0.28115		
33	Pearl	400,737	400,011	376	36	93	−0.08566	−0.63132	345,465	21,841
	Zhujiang_USGS	389,621	384,181	362	27	58	−0.04476	−1.08950		
	Zhujiang	389,567		403	44	102	0.04362	−0.71811	351,753	18,240
	Zhujiang_HR	389,567		364	17	39	−0.01094	−0.92410	320,890	4836
34	Irrawaddy	376,350		719	264	480	0.11201	−1.20837	264,082	3828
	Irrawaddy_HR	358,899		413	65	165	−0.11135	−0.71069	276,979	4149
35	Salween_USGS	375,019	260,817	412	45	104	0.09925	−0.62790		
	Salween									
36	Senegal	365,245	364,334	722	102	248	−0.01658	−0.58194	285,405	
37	Godavari	310,376		1322	174	409	−0.03582	−0.61706	46,056	139,818
	Godavari_USGS	310,376	310,057	1197	511	895	0.05789	−1.08612		
38	Krishna_USGS	258,785	258,033	1417	604	1076	0.02806	−1.23745		
	Krishna	258,703		1586	229	526	0.13806	−0.61601	25,466	95,703
39	Fraser*	248,870		235	13					
40	Thelon*	240,802		2367	107				86,080	24,323
41	Vistula_HR	192,638		28	1	3	0.00280	−0.43349	192,172	57
	Vistula	192,638		71	16	39	0.08515	−0.58334	192,622	16
42	Rhine_HR	163,012		242	14	35	0.15001	−0.55198	146,671	4020
43	Kuskokwim	142,936		129	21	53	−0.01961	−0.46811	119,884	17,528
44	Hong_USGS	138,876	126,689	515	71	179	0.00001	−0.39875		
	Hong_HR	138,856		417	17	47	−0.00924	−0.29555	106,869	1340
	Hong	138,852		359	23	69	0.02669	−0.45306	138,761	91
45	Elbe	138,383		360	89	172	−0.01386	−1.14554	94,800	3060
	Elbe_HR	138,383		523	76	188	0.01266	−0.63292	97,177	3787
46	Brazos*	137,028		131	2				137,009	
47	Oder_HR	118,790		97	10	28	0.02390	−0.17088	113,378	744
	Oder	118,731		107	18	44	−0.02836	−0.54795	112,811	0
48	Loire	118,037	118,037	309	36	97	0.13774	−0.46099	79,692	3360
49	Mobile	110,929	110,423	238	7	18	0.02147	−0.45016		
50	Po	98,772	98,772	349	84	192	−0.04637	−0.75861	74,053	1132
51	Rhone	95,895		160	24	59	−0.07300	−0.97210	82,791	709
	Rhone_HR	95,895		292	33	87	−0.14862	−0.52172	81,847	302
52	Neman	92,523		164	25	56	−0.07024	−0.91249	92,521	0
53	Garonne	82,122	82,122	173	14	31	0.05836	−0.49984	61,218	4264
54	Susquehanna*	78,773		386	4				76,694	770
55	Cauvery_USGS	78,369	78,368	2163	946	1638	0.19893	−1.14369		
	Cauvery	78,369		2775	218	495	0.05446	−0.83328	3251	0
56	Sacramento	75,501	73,348	76	2	7	−0.01000	−0.31222		
	Sacramento	72,336	71,663	85	3	8	−0.21507	−0.47397		
57	Fly_USGS	74,421	74,029	23	5	12	0.01328	−0.59074		
	Fly_HR	74,314		22	2	6	0.01240	0.02093	70,108	3572
	Fly	74,308		22	9	17	0.01053	−1.14813	56,403	16,997

(*continued on next page*)

Table 1 (*continued*)

#	River basin	Entire Drainage Basin								
		Size_all	Size_dated	Av. Age	±S.D.	Range/2	Fisher's		Sediments	Volcanics
	n = 76	km²	km²	Myr	Myr	Myr	Skewness	Kurtosis	km²	km²
58	San Joaquin	72,093	71,338	75	3	9	0.06853	−0.34742		
59	Copper									
60	Gambia	58,046	57,994	647	171	364	−0.14485	−0.64261	36,406	
61	Skeena	55,420	52,623	162	29	71	−0.02646	−0.70222		
62	Weser	44,776		147	14	36	−0.10200	−0.60907	44,226	551
	Weser_HR	44,776		135	12	24	0.01416	−1.15814	43,458	1130
63	Hudson*	41,977		706	36				27,474	79
64	San Joaquin	39,664	39,537	104	4	11	−0.03780	−0.42019		
65	Altamaha	36,532	36,532	136	49	91	−0.00412	−1.21205		
66	Hudson	33,415	33,415	988	76	170	−0.00373	−0.70357		
67	Nass	28,391	26,676	142	37	73	−0.01266	−1.10454		
68	Connecticut	27,883	27,828	472	13	32	0.00371	−0.75339	17,001	3261
69	Cagayan_USGS	27,713	27,713	44	15	34	−0.06292	−0.71006		
	Cagayan_HR	27,712		22	4	10	0.03123	−0.53438	26,305	0
	Cagayan	27,671		64	17	39	−0.03838	−0.56816	24,766	2905
70	Potomac	21,652	21,652	424	13					
71	Eel	9529	9529	115	29	53	0.09123	−1.13541		
72	Russian	3843	3843	99	20	38	0.09980	−1.09205		
73	Taunton_HR	1456								
74	Blackstone_HR	1229								
75	Pawcatuck_HR	821								
76	Pawtuxet_HR	604								

#	Entire Drainage Basin						Sampled Drainage Basin					
	Endogenous	Sediments	Volcanics	Endogenous	Other (lake, glacier, undated)		Latitude	Longitude	Size_sampled	Av. Age	±S.D.	Range/2
	km²	%	%	%	km²	%	degrees	degrees	km²	Myr	Myr	Myr
1	1,847,421	68	1	31	1978	0.03	−1.927	−55.518	4,691,148	634	148	363
	1,394,291	70	6	23	33,481	0.56	−1.927	−55.518	4,691,148	475	55	
2	1,282,760	65	0	35	53,330	1.44	−4.28	15.28	3,635,000	1057	79	
3	156,426	94	1	4	14,929	0.43						
4	125,869	95	2	4								
5	1,210,749	52	6	42	86,148	2.87	At mouth	At mouth	2,916,906	894	134	
6	338,344	74	13	13	9396	0.36	−32.94	−60.63	2,528,952	382	86	
	334,390	75	12	13	0	0.00	−32.94	−60.63	2,528,952	384	42	119
7	564,892	72	4	24	12,862	0.55	70.689	127.33	2,310,857	825	63	
8	259,047	63	26	11	14,654	0.64						
9							At mouth	At mouth	1,732,047	411	64	129
	120,914	90	3	6	5416	0.28	At mouth	At mouth	1,732,032	418	21	
10	740,297	58	1	40	5387	0.29						
11	233,452	85	2	14								
12	661,497	49	2	49	35,071	2.54	At mouth	At mouth	1,378,126	963	186	
13	184,840	79	4	17	1151	0.10						
14	215,520	68	9	23	4121	0.42	25.62	85.205	769,487	804	82	
							25.62	85.205	764,139	805	333	593
15	239,401	69	6	26	4357	0.46	18.15	−63.55	825,149	596	102	
	383,564	59	0	41	0	0.00	18.15	−63.55	825,149	697	233	436
16	241,198	70	3	29	24,999	2.93	24.735	68	853,168	398	49	
							24.735	68	848,267	311	85	164

(*continued on next page*)

Table 1 (*continued*)

#	Entire Drainage Basin						Sampled Drainage Basin					
	Endogenous	Sediments	Volcanics	Endogenous	Other (lake, glacier, undated)		Latitude	Longitude	Size_sampled	Av. Age	±S.D.	Range/2
	km^2	%	%	%	km^2	%	degrees	degrees	km^2	Myr	Myr	Myr
17	164,041	66	14	19	4821	0.60			847,642			
18							23.554	100.17	115,580	330	51	103
	55,113	91	2	7	6434	0.83	23.554	100.17	115,578	246	21	
19	65,332	84	3	8	43,457	5.52	48.2261	16.4086	101,476	434	90	224
	99,585	84	3	13	0	0.00	48.2261	16.4086	101,476	387	85	
	8715	93	2	5	502	0.31	48.2261	16.4086	158,645	206	17	
20							−35.116	139.28	774,942	149	5	16
	59,379	89	4	8	164	0.02	−35.116	139.28	774,942	192	13	
21	357,827	53	0	46	1268	0.16	At mouth	At mouth	760,273	1184	220	
	346,121	54	1	45	0	0.00	At mouth	At mouth	760,273	1133	248	579
22							37.75	118.82	760,992	278	31	68
	58,886	92	0	8	1433	0.19	37.75	118.82	760,992	366	24	
23							45.702078	−120.72971	715,064			
24							26.209	90.56	455,269	376	83	153
	203,090	65	2	32	759	0.12	26.209	90.56	458,086	576	109	
25							17.6475	95.4855	647,769	500	133	298
26	32,859	82	13	5	1295	0.20	68.676	161.29	644,451	295	12	
27	49,792	78	13	9	252	0.05						
28	50,362	90	0	10	5993	1.18	At mouth	At mouth	506,138	377	30	
29		100			1817	0.41						
30	19,782	92	3	5	781	0.18						
31	0	100	0	0	3064	0.00	At mouth	At mouth	437,313	98	16	
32							36.016265	−114.73698	164,868	728	38	102
33	32,706	86	5	8	726	0.18						
							23.04	112.45	335,594	374	32	63
	18,671	91	5	5	903	0.23	23.04	112.45	335,550	407	33	
	63,841	82	1	16	0	0.00	23.04	112.45	335,550	374	21	46
34	107,503	71	1	29	4033	1.07	17.6475	95.4855	372,033	727	249	
	69,755	77	1	19	18,599	5.18	17.6475	95.4855	354,580	418	66	161
35							16.8925	97.628333	369,434	412	42	106
							16.8925	97.628333	262,401	442	32	
36	78,929	78		22	912	0.25						
37	124,503	15	45	40	0	0.00	16.78	81.856	309,807	1325	84	
							16.78	81.856	309,807	1200	515	900
38							16.5	80.61	258,000	1423	625	1072
	137,522	10	37	53	11	0.00	16.5	80.61	258,000	1592	124	
39							At Hope	At Hope	231,247	260	20	
40	130,398	36	10	54								
41	196	100	0	0	23,069	11.98	At mouth	At mouth	192,281	28	1	4
	0	100	0	0	0	0.00	At mouth	At mouth	192,281	71	15	
42	10,497	90	2	6	1245	0.76	51.829	6.226	158,645	249	15	41
43	4845	84	12	3	678	0.47	At mouth	At mouth	123,331	133	12	
44							21.395	105.238	48,468	769	138	387
	25,809	77	1	19	4837	3.48	21.395	105.238	48,460	581	34	90
	0	100	0	0	0	0.00	21.395	105.238	48,460	358	31	
45	40,523	69	2	29	0	0.00	53.543	9.981	138,429	360	67	
	18,534	70	3	13	634	0.46	53.543	9.981	138,429	523	76	197
46	12	100		0								
47	2816	95	1	2	20	0.02	At mouth	At mouth	118,764	97	10	27
	5723	95	0	5	196	0.17	At mouth	At mouth	118,764	107	17	
48	34,984	68	3	30	0	0.00						

(*continued on next page*)

Table 1 (*continued*)

#	Entire Drainage Basin						Sampled Drainage Basin					
	Endogenous	Sediments	Volcanics	Endogenous	Other (lake, glacier, undated)		Latitude	Longitude	Size_sampled	Av. Age	±S.D.	Range/2
	km^2	%	%	%	km^2	%	degrees	degrees	km^2	Myr	Myr	Myr
49												
50	23,586	75	1	24	0	0.00						
51	11,803	87	1	12	592	0.62	44.586	4.724	69,400	165	20	
	11,784	85	0	12	713	0.74	44.586	4.724	69,400	319	35	99
52	0	100	0	0	2	0.00	At mouth	At mouth	92,420	164	24	
53	16,640	75	5	20	0	0.00						
54	1309	97.4	1	1.7			39.58	−76.1	70,162	381	4	8
55							11.338	79.711	78,325	2167	960	1642
	75,116	4	0	96	2	0.00	11.338	79.711	78,325	2780	336	
56												
57							At mouth	At mouth	62,663	23	5	11
	102	94	5	0	532	0.72	At mouth	At mouth	62,658	26	2	7
	877	76	23	1	31	0.04	At mouth	At mouth	62,653	24	5	
58												
59							60.67339	−144.75514	61,852	134	12	
60	21,587	63	37		53	0.09						
61												
62	0	99	1	0	0	0.00	At mouth	At mouth	44,728	147	15	
	188	97	3	0	0	0.00	At mouth	At mouth	44,728	135	12	23
63	14,339	65.4	0.2	34.2	86	0.2						
64												
65												
66							43.248799	−73.831963	7126	1261	102	256
67												
68	7621	61	12	27								
69									27,773	39	15	32
	1407	95	0	5	0	0.00	At mouth	At mouth	27,771	23	4	11
	0	90	10	0	0	0.00	At mouth	At mouth	27,771	64	14	
70							39.304114	−79.312363	189	313	7	12
71												
72												
73							41.88290	−71.09080	950	438	37	67
74							41.89900	−71.39055	1142	696	63	151
75							41.39177	−71.83908	1142	630	65	142
76							41.76720	−71.39577	950	468	30	67

#	Sampled Drainage Basin										
	Fisher's		Sediments	Volcanics	Endogenous	Sediments	Volcanics	Endogenous	Other (lake, glacier, undated)		
	Skewness	Kurtosis	km^2	km^2	km^2	%	%	%	km^2	%	
1	0.02570	−0.73578	3,472,457	69,095	1,147,619	74.0	1.5	24.5	1978	0.04	
			3,598,882	180,388	889,962	77.1	3.9	19.1	21,916	0.47	
2			2,323,236	6302	1,252,332	64.9	0.2	35.0	53,129	1.46	
3											
4											
5			1436,617	183,450	1,210,691	50.8	6.5	42.8	86,148	2.95	
6			1,848,722	332,322	338,771	73.4	13.2	13.4	9138	0.36	
	0.03653	0.29443	1,874,594	322,543	331,815	74.1	12.8	13.1	0	0.00	

(*continued on next page*)

Table 1 (*continued*)

#	Sampled Drainage Basin										
	Fisher's		Sediments	Volcanics	Endogenous	Sediments	Volcanics	Endogenous	Other (lake, glacier, undated)		
	Skewness	Kurtosis	km^2	km^2	km^2	%	%	%	km^2	%	
7			1,632,436	101,183	564,918	71.0	4.4	24.6	12,320	0.53	
8											
9	0.06262	−1.17537	1,715,216	0	0	99.0	0.0	0.0	16,831	0.97	
			1,573,390	61,631	92,087	91.1	3.6	5.3	4925	0.28	
10											
11											
12			655,404	26,174	661,476	48.8	1.9	49.3	35,071	2.54	
13											
14			516,194	86,468	166,825	67.3	11.3	21.8	3003	0.39	
	0.05428	−1.28218	669,826	73,763	8519	87.7	9.7	1.1	12,031	1.57	
15			580,049	23,668	218,625	70.5	2.9	26.6	2807	0.34	
	0.06822	−1.24964	538,088	2119	284,942	65.2	0.3	34.5			
16			581,835	26,290	241,219	70.2	3.2	29.1	24,868	2.91	
	0.06653	−1.08537	717,629	0	90,830	84.6	0.0	10.7	39,808	4.69	
17											
18	0.03011	−1.17775	115,580	0	0	100.0	0.0	0.0			
			109,512	0	6065	94.8	0.0	5.2		0.00	
19	−0.06845	−0.58606	86,366	120	14,732	85.1	0.1	14.5	428	0.42	
			79,995	0	21,481	78.8	0.0	21.2		0.00	
			146,691	2739	8713	92.8	1.7	5.5	502	0.32	
20	−0.07586	−0.34672	773,230	0	0	99.8	0.0	0.0	1712	0.22	
			686,061	29,293	59,424	88.5	3.8	7.7	164	0.02	
21			402,729	2796	354,748	53.0	0.4	46.7	0	0.00	
	−0.09501	−0.73498	407,243	9128	343,902	53.6	1.2	45.2			
22	−0.07367	−0.99691	760,858	0	0	100.0	0.0	0.0	134	0.02	
			700,739	0	58,837	92.3	0.0	7.7	1415	0.19	
23											
24	−0.01579	−1.15662	412,326	0	6518	90.6	0.0	1.4	36,425	8.00	
			274,885	13,670	168,790	60.1	3.0	36.9	741	0.16	
25	0.00140	−0.71051	349,327	6611	7979	53.9	1.0	1.2	283,852	43.82	
26			528,719	82,000	32,858	82.2	12.7	5.1	874	0.14	
27											
28			449,833	0	50,362	89.9	0.0	10.1	5943	1.17	
29											
30											
31			434,249	0	0	100.0	0.0	0.0	3064	0.70	
32	0.05366	−0.45725									
33											
	0.01904	−1.08450	330,152	0	0	98.4	0.0	0.0	5442	1.62	
			305,321	18,230	11,437	91.1	5.4	3.4	563	0.17	
	0.03089	−0.95914	287,470	4340	43,740	85.7	1.3	13.0		0.00	
34			259,796	3828	107,472	70.6	1.0	29.2	4033	1.08	
	−0.64790	−0.74144	272,703	4149	69,722	76.9	1.2	19.7	18,590	5.24	
35	−0.04241	−0.81311	247,784	0	4774	67.1	0.0	1.3	116,875	31.64	
			210,179	0	52,000	81.0	0.0	20.0	2861	1.09	
36											
37			45,274	139,975	124,558	14.6	45.2	40.2		0.00	
	−0.01344	−1.23027	175,761	133,727	0	56.7	43.2	0.0	319	0.10	
38	0.02610	−1.19888	159,204	98,064	0	61.7	38.0	0.0	733	0.28	
			24,527	95,821	137,652	9.5	37.1	53.4		0.00	
39							35.8	42.3	15		

(*continued on next page*)

Table 1 (*continued*)

#	Sampled Drainage Basin									
	Fisher's		Sediments	Volcanics	Endogenous	Sediments	Volcanics	Endogenous	Other (lake, glacier, undated)	
	Skewness	Kurtosis	km^2	km^2	km^2	%	%	%	km^2	%
40										
41	−0.06291	−0.04339	168,981	57	195	87.9	0.0	0.1	23,048	11.99
			192,262	19	0	100.0	0.0	0.0		0.00
42	0.01342	−0.51266	143,028	4022	10,488	90.2	2.5	6.6	1244	0.78
43			108,969	9766	4099	88.7	8.0	3.3	498	0.40
44	−0.05296	−0.45334	46,723	0	0	96.4	0.0	0.0	1745	3.60
	0.03565	−0.27638	32,532	225	11,924	67.1	0.5	24.6	3779	7.80
			48,371	89	0	99.8	0.2	0.0		0.00
45			94,823	3064	40,542	68.5	2.2	29.3		0.00
	−0.11573	−0.50716	115,801	3786	18,542	83.7	2.7	13.4	628	0.45
46										
47	−0.08466	−0.21431	115,188	746	2810	97.0	0.6	2.4	20	0.02
			112,851	0	5713	95.2	0.0	4.8	200	0.17
48										
49										
50										
51			58,111	366	10,387	84.4	0.5	15.1	537	0.77
	0.06296	−0.15437	59,297	113	9344	85.4	0.2	13.5	714	1.03
52			92,420	0	0	100.0	0.0	0.0		0.00
53										
54	0.06391	−0.52713								
55	−0.05493	−1.14010	78,325	0	0	100.0	0.0	0.0		0.00
			3126	0	75,200	4.0	0.0	96.0		0.00
56										
57	−0.01506	−0.88293	62,418	0	0	99.6	0.0	0.0	246	0.39
	0.00947	−0.26870	59,593	2429	103	95.1	3.9	0.2	533	0.85
			47,728	14,043	882	76.2	22.4	1.4	10	0.02
58										
59			24,750	15,711	10,511	48.6	30.8	20.6	10,880	17.59
60										
61										
62			44,182	546	0	98.8	1.2	0.0		0.00
	0.01203	−1.08314	43,415	1125	188	97.1	2.5	0.4		0.00
63										
64										
65										
66	0.01466	−0.65088								
67										
68										
69	−0.09882	−0.77218	27,773	0	0	100.0	0.0	0.0		0.00
	0.03133	−0.43840	26,335	0	1436	94.8	0.0	5.2	0	0.00
			24,863	2908	0	89.5	10.5	0.0		0.00
70	−0.01468	−1.11363								
71										
72										
73	−0.02440	−1.17730	671	0	279	70.7	0.0	29.3		0.0
74	0.16802	−0.75694	112	1	1010	9.9	0.1	89.2	10	0.8
75	0.09050	−0.87856	42	0	688	5.7	0.0	92.2	16	2.1
76	0.00468	−0.65866	65	0	482	11.3	0.0	83.8	28	4.9

stratigraphic sub-divisions suffer the most from the assumption of rectangular distributions of likely average ages between upper and lower age boundaries. The bias is particularly large for river basins with large areas of undifferentiated Precambrian or Archean bedrock units whose average ages are also strongly affected by the assumption of the oldest age of rocks occurring in such basins. For example, setting the lower age boundary of Archean units in the Cauvery River basin (India) to the canonical 4000 million years (Plumb, 1991; Van Kranendonk, 2012), the average bedrock age of the Cauvery drainage basin is 2775 ± 352 million years. If, however, this age is adjusted to the oldest geochronologically-dated units in the Cauvery river basin, the Gorur TTG gneisses and associated rocks (3340 million years) of the Dharwar craton (Jayananda et al., 2015), the average bedrock age of this basin decreases by 250 million years to 2524 ± 220 million years. Average bedrock ages correlate well ($r^2 > 0.7$) with the spatial abundance of igneous and metamorphic bedrock in watersheds, are anti-correlated ($r^2 > 0.8$) with the abundance of sedimentary bedrock in watersheds, and show no correlation with the abundance of volcanic bedrock in watersheds (not shown). While the latter finding is somewhat surprising given the lower survival probability of rocks emplaced at or near the surface (Wilkinson et al., 2009), the low spatial abundance of volcanic bedrock in general likely obscures clear age relationships at the watershed scale. These systematics confirm well known bedrock age relationships for these broadly defined lithologic units (e.g. Peucker-Ehrenbrink and Miller, 2007b and references therein; Wilkinson et al., 2009).

3. Bias and bias corrections

3.1. The flux and $^{87}Sr/^{86}Sr$ of continental strontium to seawater

The average Sr concentration and $^{87}Sr/^{86}Sr$ of continental runoff have been assessed in slightly different ways. The most basic approach of determining average values is to multiply Sr concentration with water flux and isotope composition to estimate a flux-weighted Sr isotope composition that can be scaled to the global river discharge (e.g. Goldstein and Jacobsen, 1987). Using this approach for all analyzed rivers that collectively deliver one quarter of the global runoff, the global average Sr concentration and isotope composition is 0.71 ± 0.06 μM and 0.7101 ± 0.0005 (Goldstein and Jacobsen, 1987). The fundamental problem with this approach is that more data is available for large rivers that, when scaled up, exert a disproportionate influence on the global mass balance – a problem known as the "Amazon effect" (Meybeck, 1988, p. 253). This problem can be avoided by using regional averages that take into account certain characteristics of the global drainage. Regions can be defined based on geomorphic, climatic, regional or lithologic characteristics, or combinations thereof (e.g., Palmer and Edmond, 1989). Using a variant of this approach, Peucker-Ehrenbrink et al. (2010) investigated large-scale drainage regions according to boundaries delineated by Graham et al. (1999, 2000). The data for rivers in each drainage region can be extrapolated to the total discharge from each region based on the most comprehensive dataset of rivers available (Land2Sea database, Peucker-Ehrenbrink, 2009, 2018, supplemented by data in Milliman and Farnsworth, 2011, Fig. 3). It is worth noting that most rivers have not been analyzed in time-series fashion and literature data for individual rivers may therefore be biased. Applied to half of the global runoff, this approach yields an average Sr concentration of 1.2 μM (4.7×10^{10} mol yr^{-1}) and $^{87}Sr/^{86}Sr$ of 0.7111. While this $^{87}Sr/^{86}Sr$ value is similar to previous estimates (0.7114: Palmer and Edmond, 1989; 0.7116: Davis et al., 2003; 0.71144: Vance et al., 2009), the Sr concentration is significantly higher than previous estimates (0.71–0.92 μM, Goldstein and Jacobsen, 1987; Palmer and Edmond, 1989).

The above approach largely avoids the "Amazon effect". However, it does not eliminate all biases, as regional averages are still biased towards larger river systems that often have different characteristics than smaller systems (e.g. Milliman and Syvitski, 1992). In addition, many rivers have only been sampled once or twice (e.g. Gaillardet et al., 1999), and it is unclear how representative these values are. Temporal biases can be significant in systems with very dynamic hydrographs. This can be demonstrated for the Fraser River in British Columbia (Fig. 4) where previous near-mouth sampling yielded two $^{87}Sr/^{86}Sr$ values for the river in late spring (May: Wadleigh et al., 1985, exact sampling date could not be reconstructed) and summer (July: Cameron and Hattori, 1997, exact sampling date could not be reconstructed). Time-series data from the Fraser River Observatory on the lower Fraser River (Voss et al., 2014) illustrate how the isotopic composition of the

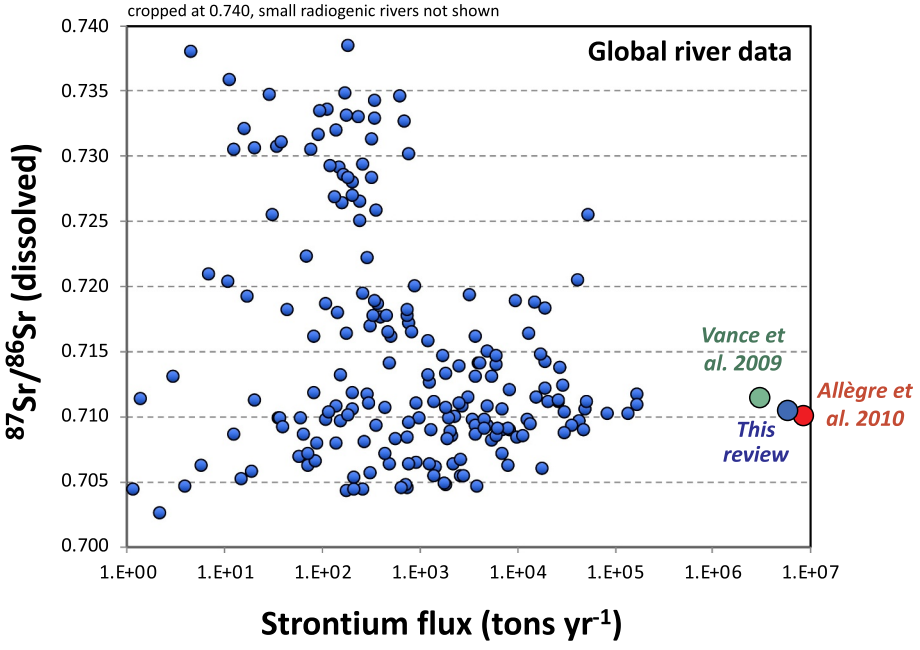

Fig. 3. Data on dissolved $^{87}Sr/^{86}Sr$ and Sr flux for individual rivers together with global estimates of the terrestrial delivery of Sr to the ocean. Note that the $^{87}Sr/^{86}Sr$ axis is cropped at 0.740, eliminating some smaller radiogenic rivers from the display.

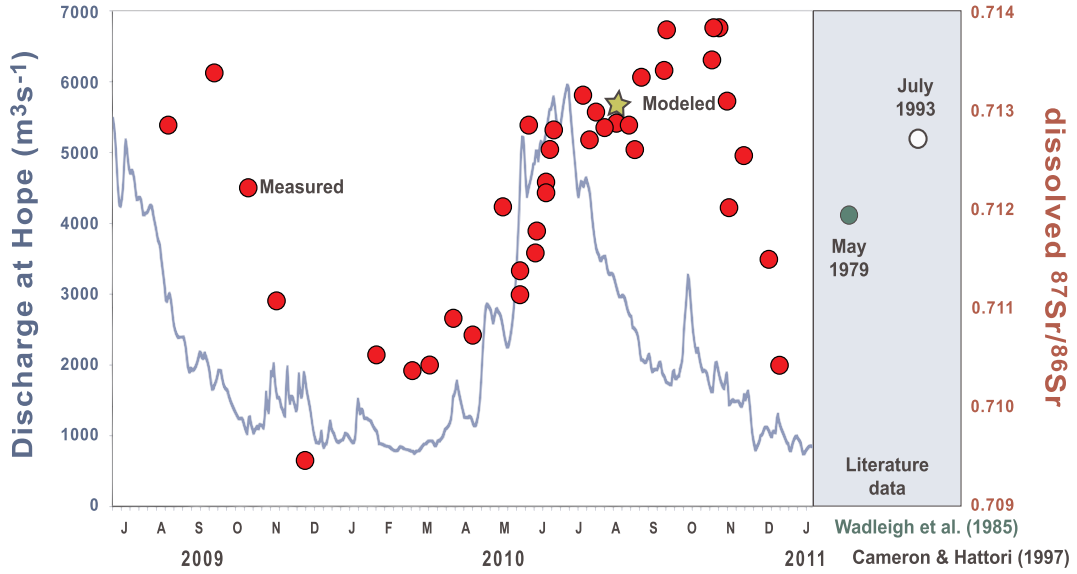

Fig. 4. Dissolved $^{87}Sr/^{86}Sr$ (red circles, Voss et al., 2014) in the Fraser River near its mouth. Literature data (green circle: Wadleigh et al., 1985; white circle: Cameron and Hattori, 1997) are shown in the gray field on the right without discharge information, because the sampling dates could not be reconstructed. Fraser River discharge at Hope, B.C., Canada, is shown as blue line for 2009–2011. For details, including modeling riverine dissolved $^{87}Sr/^{86}Sr$, see Voss et al., 2014.

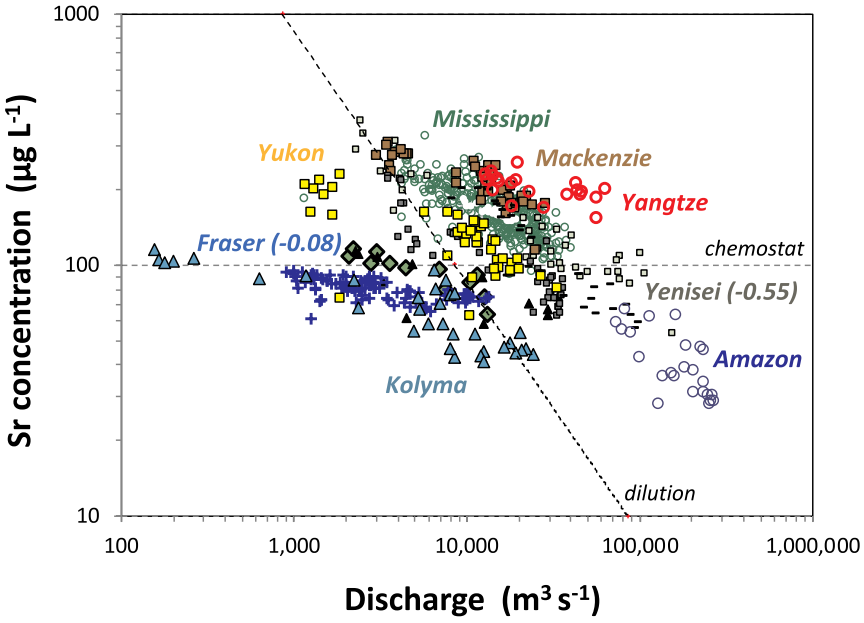

Fig. 5. Strontium concentration as a function of discharge for the Mississippi (red circles, annual averages as white circles), Fraser (blue crosses, shallowest linear trend), Salween (green diamonds), Irrawaddy (black triangles), Kolyma (blue triangles), Lena (buff-colored squares), Mackenzie (brown squares), Ob (gray squares), Yenisey (brown small rectangles, steepest linear trend) and Yukon (yellow squares) rivers. The theoretical dilution trend (black stippled line with negative slope) indicates the inability to mobilize any additional Sr as discharge increases. The theoretical case of no kinetic limitation to mobilizing Sr to keep concentrations constant as discharge increases (chemostat) corresponds to horizontal trends in the data. Data for glacial discharge in Greenland (not shown) plots in a cluster more than one order of magnitude in concentration below the low-discharge end of the Kolyma trend. Numbers in parenthesis for the Fraser and Yenisei rivers indicate exponents of the power law relationship.

river responds to the cyclic changes in the basin's hydrology, and allows to place previously published data in proper hydrologic context. Existing time series data for Sr concentrations show that they vary with discharge (Fig. 5). For instance, time-series data for the Amazon (Seyler and Boaventura, 2003; Seyler, 2017, pers. comm.), Mississippi (USGS, St. Francisville), Fraser (Voss et al., 2014), Salween and Irrawaddy rivers (Chapman et al., 2015), Brahmaputra (Rai and Singh, 2007), Yangtze (Luo et al., 2014), and the large Arctic rivers (www.arcticgreatrivers.org/data.html, downloaded 11-23-2016) illustrate kinetic limitations (Godsey et al., 2009) to the mobilization of dissolved Sr as discharge increases. Power law exponents of the log-log correlations vary from −0.079 ($r^2 = 0.37$) for the Fraser River to −0.546 ($r^2 = 0.86$) for the Yenisei River, indicating that doubling discharge causes a decrease in Sr concentration by as little as 5% (Fraser) to as much as 32% (Yenisei).

Another more subtle, but nevertheless potentially important bias is related to sampling locations. Rivers are often sampled far upstream of the tidal influence, sometimes hundreds of kilometers inland. For instance, the classic gauging station on the Amazon at Óbidos is ~800 km upstream of the coast (Fig. 6) and represents only ¾ of the total drainage basin. Coastal drainages are generally underrepresented in global river flux studies (Palmer and Edmond, 1989). This can lead to bias if the makeup (lithology, runoff, specific Sr flux) of coastal areas differs from the basin average. Data from the Fraser River in western Canada show the potential magnitude of this bias (Voss et al., 2014). The gauging station at Hope, B.C., at the eastern end of the lower Fraser River valley often serves as the most seaward location for chemical data for the Fraser River. This station is outside of the tidal range that influences the Fraser at least up to the city of Mission, approximately 150 km east of the delta at Vancouver. Regional sampling of tributaries that enter the Fraser River downstream of Hope shows that unradiogenic runoff from the humid Coast Range, particularly the

Fig. 6. Amazon River basin (yellow outline) without the Tocantins River basin in the Southeast. The sampling location at Óbidos is shown as a green circle with its upstream drainage area shown in light blue. This upstream drainage area accounts for about 80% of the total Amazon River basin area and ~90% of the annual precipitation in the basin.

Harrison River with a $^{87}Sr/^{86}Sr$ of ~0.704, is neglected by using the Hope station as a representative sampling location for the Fraser River. About 15% of the total runoff of the Fraser River is neglected by using data from the Hope station as representative of the Fraser River, and the missing fraction of the total runoff is dominated by unradiogenic runoff from the young, volcanically active Coast Range with $^{87}Sr/^{86}Sr$ values of 0.704–0.705 (Voss et al., 2014). This bias is also reflected in the slightly older average bedrock ages of the basin above Hope (260 ± 20 Myr, 1 s.d.) compared to the entire drainage basin (235 ± 13 Myr, 1 s.d.) Such biases are typical for larger river systems, particularly along active continental margins, where river systems tend to break through Coast Mountains to drain portions of the adjacent, often geologically older, continental interior.

It has been shown that the average bedrock geology of individual river basins and larger drainage regions correlates quasi-linearly with the dissolved riverine $^{87}Sr/^{86}Sr$ (Peucker-Ehrenbrink et al., 2010; Fig. 7). These correlations can be approximated with straight lines because the slight curvature resulting from the exponential term of radioactive decay equation can be linearized by Taylor Series expansion if the time periods considered are short compared to the ~49.6 billion year half-life of ^{87}Rb (Rotenberg et al., 2012). Typical bedrock ages of hundreds of millions of years meet this criterion. In the following we expand previous analyses of large drainage regions to the bedrock geology of 56 river drainage basins with some of the largest Sr fluxes to the ocean. This analysis neglects the fact that not all bedrock contributes equally to the Sr flux. Such an expanded analysis would require weighting bedrock according to precipitation and the propensity of different bedrock lithologies to contribute Sr to the dissolved riverine load (Tardy et al., 1989; Gibbs et al., 1999). While these additional factors can be quantified for the present, estimating precipitation and bedrock lithology at sufficient spatial and temporal resolution for the geologic past is currently not possible.

3.2. Discussion

North America is particularly susceptible to spatial biases, because its onion-like structure of bedrock ages causes a trend towards younger geologic terrains near the coasts (Wilson, 1949; Gastil, 1960). Contributions from these younger coastal terrains tend to be underrepresented in estimates of discharge and continent-derived chemical fluxes that are based on data for 48 (67 including the Canadian Arctic Archipelago [CAA]) rivers that account for about one quarter of the global data set. The resulting bias can be illustrated by comparing river drainage basin sizes, dissolved $^{87}Sr/^{86}Sr$ and specific Sr yields (Fig. 8) of basins that are part of the large-scale drainage region that is potentially most significantly biased: the active margin along the North American West Coast. There, large rivers whose drainage basins reach beyond the Coast Range (e.g. Yukon, Fraser, Columbia, Colorado rivers, red circles

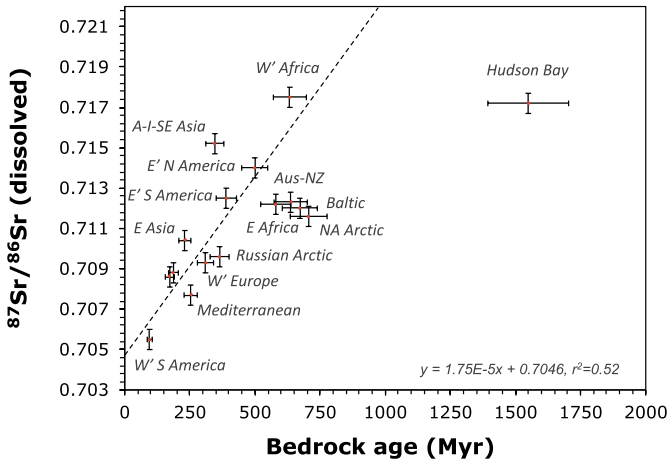

Fig. 7. Correlation between dissolved $^{87}Sr/^{86}Sr$ and average bedrock age for large-scale drainage regions, updated from Peucker-Ehrenbrink et al. (2010). Note that the linear least square fit with uncertainties in both coordinates including covariance (Reed, 1992, 2010) that yields the relation y = [2.15 ± 0.20]E-5 x + [0.7037 ± 0.0006] (95% confidence interval) assumes uncertainties of 20% in average bedrock ages and 0.0006 in dissolved $^{87}Sr/^{86}Sr$.

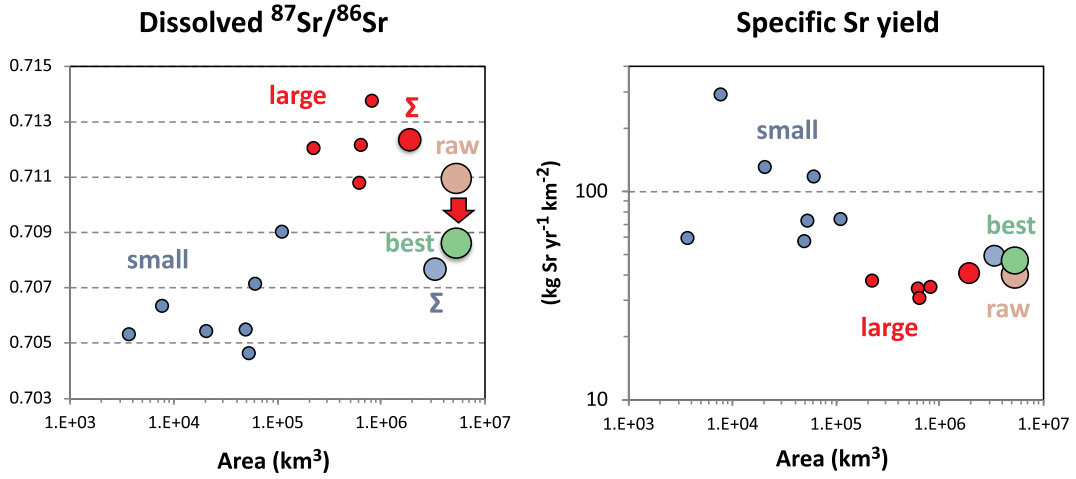

Fig. 8. Correlation of dissolved $^{87}Sr/^{86}Sr$ (a) and the specific Sr yield (b) versus size of the respective drainage basins along western North America. Large rivers draining the continental interior (red circles) are contrasted with small drainage basins that exclusively drain the western side of the Coast Range and adjacent coastal plains (red squares; Peucker-Ehrenbrink, 2009; Peucker-Ehrenbrink et al., 2010). The sums of the raw data for both types of river systems are shown in medium-sized blue and red circles (labeled "Σ"). Averaging such raw data yield a regional average shown as pink large circle (labeled "raw"). Averaging by correcting for sampling bias yields a more appropriate regional average that is shown as a green circle (labeled "best").

in Fig. 8) are more radiogenic than smaller river systems that exclusively drain the Coast Range (blue circles in Fig. 8). These include many small, mountainous river systems (Milliman and Syvitski, 1992) along the humid northern part of the Coast Range that have not been systematically investigated. Existing data for these systems indicate that they have lower dissolved $^{87}Sr/^{86}Sr$ values (0.7069) and slightly lower Sr concentrations (107 μg L^{-1}), but higher specific Sr yields than the large systems that also drain the drier continental interior (138 μg L^{-1}, 0.7123). This bias can be corrected by subtracting the Sr flux that is associated with the sampled area of the four large drainage basins (Yukon, Fraser, Columbia, Colorado) from the area of the North American West Coast drainage region. Data for some of the smaller basins can then be extrapolated to the remainder of this drainage region that includes unsampled coastal areas of the large drainage basins. Together with the Sr flux for the four large basins this correction yields an average dissolved Sr concentration of 115 μg L^{-1} with a $^{87}Sr/^{86}Sr$ of 0.7086 for the entire North American West Coast drainage (large green circle in Fig. 8). These values differ from those computed by scaling up from all existing data without taking the above bias into account (128 μg L^{-1}, 0.7109; Peucker-Ehrenbrink et al., 2010, large pink circle in Fig. 8). Such corrections for small coastal drainages address concerns that regional flux-weighted averages, for example in Alaska (0.7098, Bataille et al., 2014), can significantly differ from that of large rivers draining such regions (in Alaska e.g. Yukon River: 0.7126 modeled vs. 0.7137 measured; Bataille et al., 2014).

Several other large-scale drainage regions merit closer inspection regarding biases, among them East Africa. Data for this region is dominated by the Zambezi River (146 μg L^{-1}, 0.7239) that drains an unusually old portion of this region. A more appropriate dissolved Sr concentration and $^{87}Sr/^{86}Sr$ for this region can be computed based on the sum of the Zambezi watershed and the remainder of the region. This approach yields a revised dissolved Sr concentration of 163 μg L^{-1} with a $^{87}Sr/^{86}Sr$ of 0.7123 compared to uncorrected values of 148 μg L^{-1} and 0.7221. The large drainage area of Arabia, India, and SE Asia that is dominated by the Indus, Ganges and Brahmaputra rivers can be treated similarly and yields respective corrected Sr concentrations and $^{87}Sr/^{86}Sr$ of 102 μg L^{-1} and 0.7152 compared to uncorrected values of 103 μg L^{-1} and 0.7174. Significant future revisions may be required for the North American Arctic drainage region despite the addition of a new average for 19 smaller watersheds that drain the CAA (Brown et al., submitted). New data for the CAA balance the geochemical influence of the Mackenzie River that drains large portions of the southern part of this drainage region. However, Greenland also contributes to this large-scale drainage region, as it does to the drainage region of Eastern North America. Greenland is currently only represented in our database by a few small, Sr-poor rivers with very diverse $^{87}Sr/^{86}Sr$ (0.71 to 0.94; Goldstein and Jacobsen, 1987; Hagedorn and Hasholt, 2004; Hindshaw et al., 2014; Scribner et al., 2015), despite the fact that Greenland generates ice sheet and tundra runoff equivalent of the annual discharge of a large Arctic river (429 km^3 yr^{-1}: Mernild et al., 2009; 416 ± 57 km^3 yr^{-1}: Bamber et al., 2012; see also Rink, 1863). The geologic complexity, ice cover and scarce data currently limit our ability to predict Greenland's average dissolved Sr flux and $^{87}Sr/^{86}Sr$. This lack of data may require future revisions of Sr inputs to seawater from the two large-scale regions that include parts of Greenland.

Although the current analysis achieves resolution at the scale of individual drainage basins and therefore improves prior estimates of large scale drainage regions (Peucker-Ehrenbrink et al., 2010), significant spatial variability in the flux and isotopic composition of Sr occur within individual drainage basins (e.g. Voss et al., 2014). Although implementing a higher resolution analysis for the global terrestrial drainage is beyond the scope of this study, the Nile basin illustrates such biases well, as it shows strong regional gradients in rainfall (Fig. 9; northern deserts: light blue, wet southern highlands: dark blue) and bedrock geology (Precambrian Nubian desert in the Northeast, Quaternary to Neogene volcanic rocks of the Afar Rift system in the southeast). While the non-weighted average bedrock age of the Nile drainage basin is 871 ± 184 million years, the average bedrock age weighted according to average annual rainfall is 644 ± 199 million years. The 227 million years younger weighted bedrock age reflects higher rainfall in the geologically younger terrains. It is conceivable that the contrast is even larger if the analysis were extended to include specific Sr yields that are likely higher in young volcanic terrains than in Precambrian basement.

With all the corrections discussed above, we compute a best estimate of the globally weighted (by Sr flux) dissolved Sr concentration and $^{87}Sr/^{86}Sr$ of 1.2 μM (104 μg L^{-1}) and 0.71106 for continental runoff. This estimate includes contributions from small islands of Oceania (Table 2). Spatial variations of bedrock ages, runoff, suspended sediment yield, strontium yield, strontium concentration and dissolved $^{87}Sr/^{86}Sr$ at the scale of large-scale drainage regions are graphically summarized in Fig. 10 in form of cartograms (Gastner and Newman, 2004).

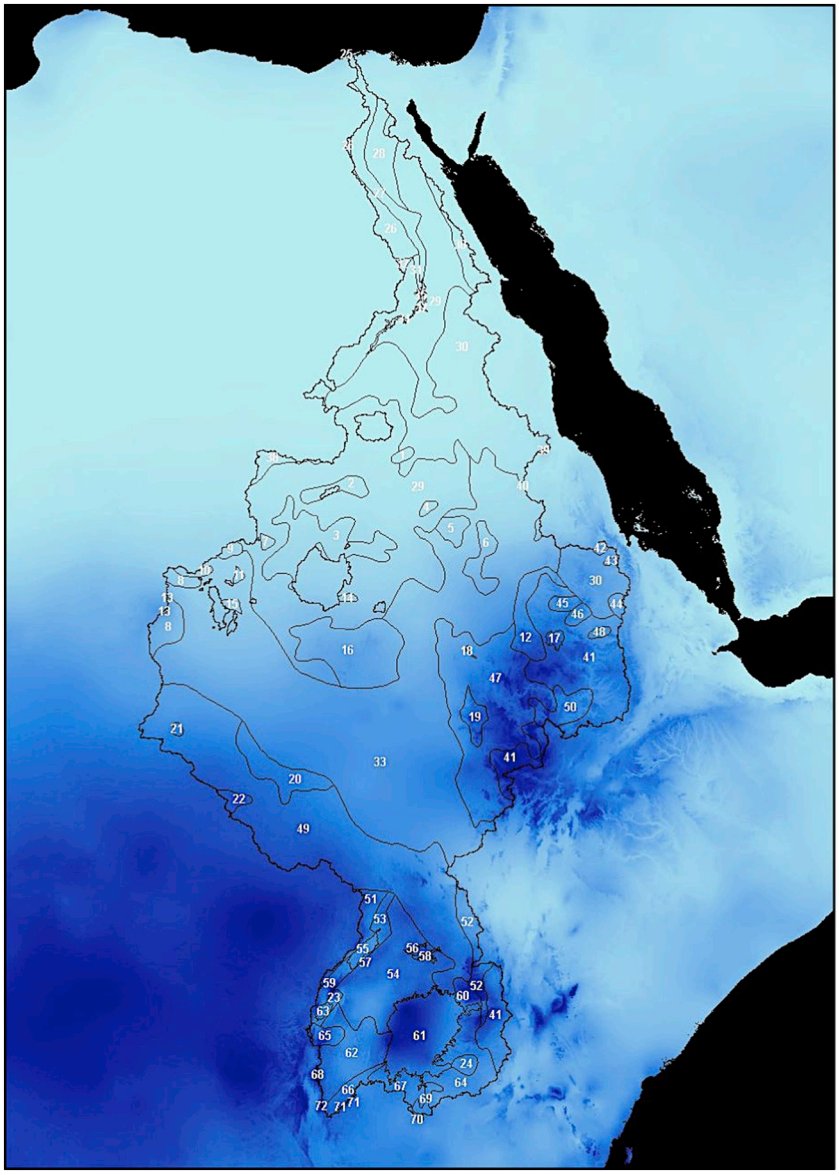

Fig. 9. Color-coded map of the Nile drainage basin according to average annual precipitation. The intensity of the blue indicates intensity of average annual rainfall. Variability in bedrock geology across the basin is not shown.

4. Other continental sources of strontium to seawater

4.1. Submarine groundwater discharge

Continental inputs to seawater are not restricted to river discharge. Submarine groundwater discharge (SGD) along the coasts and reactions in estuarine salinity gradients have been well documented, and their potential impact on the marine $^{87}Sr/^{86}Sr$ record has been discussed (Chaudhuri and Clauer, 1986; Basu et al., 2001; Allègre et al., 2010; Beck et al., 2013; Trezzi et al., 2016). Beck et al. (2013) have made the most comprehensive assessment of Sr inputs from SGD, including an attempt at a global flux estimate. As the present-day $^{87}Sr/^{86}Sr$ of this end-member (0.7089) is only slightly less radiogenic than modern seawater (0.70918), the overall effect of the SGD Sr flux ([0.7 to 2.8] $\times 10^{10}$ mol y^{-1}) on the marine Sr isotope budget is small. The range of estimated fluxes is similar to that of Chaudhuri and Clauer (1986: 1.94×10^{10} mol y^{-1}), but less radiogenic in its composition (Chaudhuri and Clauer, 1986: $^{87}Sr/^{86}Sr = 0.711$). Reports of significant regional, and by inference global, impacts of submarine groundwater fluxes from the Ganges-Brahmaputra delta on the Bay of Bengal (Basu et al., 2001) are very difficult to reconcile with measured Sr concentrations and isotope ratios reported from salinity gradients in the Bay of Bengal. The notion of a high SGD Sr flux from this region has also been criticized because the permeability of the Bengal Basin sediments and hydrologic head are apparently too small to sustain such a large flux (Harvey, 2002; Basu et al., 2002). Strontium data (Beck et al., 2013) from a salinity transect in the northern Bay of Bengal, the Sandwip Channel in the northern Bay of Bengal, and a salinity transect in a distributary channel of the G-B (Meghna) river system are consistent with G-B river water compositions at salinities greater than ~15. Only two low salinity samples require either higher Sr concentrations or more radiogenic composition than G-B river water usually provide, and could indicate limited contributions from groundwaters (Fig. 11). Beck et al. (2013) also document evidence for isotope exchange between meteoric- and marine-derived Sr that can cause non-conservative mixing in estuaries. Such Sr isotope exchange flux will likely vary over time as a function of sea level and paleogeography (Chaudhuri and Clauer, 1986). For the purpose of this review we gauge the global impact of the SGD flux and isotope composition on the Sr budget of seawater by using the average freshwater SGD Sr flux and $^{87}Sr/^{86}Sr$ as estimated by Beck et al. (2013).

Table 2

Abbreviations are as follows: A_T, total exorheic drainage area, corrected for internal drainages according to Peucker-Ehrenbrink (2009); T_e, average bedrock age of the exorheic land area according to Peucker-Ehrenbrink et al. (2010); Seds., percentage of sedimentary bedrock cover; Extr., percentage of extrusive bedrock cover; Endog., percentage of endogenous (intrusive and metamorphic) bedrock cover according to Peucker-Ehrenbrink et al. (2010); A_b, best estimate of the exorheic drainage area represented in the Land2Sea database; N, number of river basins represented in the Land2Sea database; A%, percentage of exorheic land area represented in the Land2Sea database; Q_b SS, best annual suspended sediment flux estimate based on data in the Land2Sea database; N, number of rivers with suspended sediment flux information in the Land2Sea database; Q SS%, percentage of the exorheic land area in the Land2Sea database (A_b) for which sediment fluxes have been characterized; Q_{AT} SS, Q_b SS extrapolated to total exorheic land area for a given drainage region (A_T); Y SS, average annual suspended sediment yield; D, average denudation rate; Q_b, best estimate of the annual water flux based on data in the Land2Sea database; N, number of rivers with water flux estimates in the Land2Sea database; Q %, percentage of exorheic land area represented in the Land2Sea database that has been characterized regarding water fluxes; Q_{AT}, Q_b extrapolated to total exorheic land area (A_T); R, average runoff; c Sr_d, average concentration of dissolved Sr in rivers, weighted by water flux and dissolved Sr concentration of rivers represented in the Land2Sea database; $^{87}Sr/^{86}Sr_w$, average dissolved $^{87}Sr/^{86}Sr$ of rivers represented in the Land2Sea database, weighted according to dissolved Sr concentration and water flux. A_b Sr, drainage area for which riverine Sr isotope data are available in the Land2Sea database; % total, percentage of A_b Sr relative to total drainage area represented in the Land2Sea database (A_b); Q_b, best annual water flux of exorheic drainage areas with information on Sr isotope composition; % total, percent of total annual water flux (Q_{AT}) that has been characterized for Sr isotopes; N, number of rivers characterized for Sr isotopes; Q Sr, annual Sr flux per exorheic drainage area. Values in italics have been corrected for regional biases (see main text). Oceania, a representation of smaller ocean islands that are not part of larger drainage regions. We distinguish between to sum of all areas (Sum), the sum of properties of exorheic drainages (Sum exorheic), and the exorheic sum that includes Oceania. T_{ew}, average weighted (by property, e.g. area, annual suspended sediment flux, annual water flux) bedrock age of the exorheic drainage. Note that weighted bedrock ages of area-related properties are older (~450 Myr) compared to water flux-related (~400 Myr) and suspended sediment-related (~310 Myr) properties. % Sediments, Extrusives and Endogenous, fraction of sedimentary, extrusive and endogenous bedrock, weighted according to different properties (e.g. area, suspended sediment flux, water flux).

ID	Drainage Region	A_T	T_e	Seds.	Extr.	Endog.	A_b	N	A%	Q_b SS	N	Q SS%	Q_{AT} SS	Y SS
		km^2	Myr	%	%	%	km^2			$Mt\ yr^{-1}$			$Mt\ yr^{-1}$	$t\ km^{-2}\ yr^{-1}$
1	Russian Arctic	13,087,208	364	80.3	6.9	12.8	11,799,090	50	90	94	26	87.7	107	8
2	N′ American Arctic	3,577,966	706	79.9	3.7	16.5	3,056,082	53	85	359	11	70.5	510	143
3	E′ North America	9,325,220	499	73.0	8.2	18.8	8,064,995	172	87	563	63	70.3	801	86
4	W′ Europe	1,998,839	310	65.0	6.1	28.9	1,661,020	267	83	63	76	63.6	100	50
5	E′ South America	16,369,568	390	66.3	9.5	24.2	14,650,971	132	99	1436	70	83.0	1731	106
6	W′ Africa	11,261,691	634	63.9	1.8	34.4	10,253,160	108	91	282	36	76.2	369	33
7	E′ Africa	5,701,908	637	56.8	9.6	33.6	5,106,389	90	90	194	23	40.1	775	136
8	Arabia-India-SE Asia	9,590,213	346	69.2	9.5	21.3	6,410,290	134	67	2511	57	56.7	4143	432
9	East Asia	14,073,715	231	72.3	14.2	13.4	10,558,050	301	75	2185	134	61.5	3553	252
10	W′ North America	5,405,659	173	47.4	35.0	17.6	4,145,017	175	77	626	89	63.7	1523	282
11	W′ South America	1,220,853	96	38.0	37.3	24.7	740,652	101	61	63	6	5.1	1244	1019
12	Australia-NZ	4,701,839	580	79.5	5.1	15.4	3,847,267	229	82	252	130	42.8	589	125
13	Antarctica (≥60°S)	1523,722		29.0	22.7	48.4								
14	Mediterranean	5,726,983	253	77.9	4.6	17.6	4,297,630	159	75	536	111	68.8	778	136
15	Caspian Sea	8,049,943		93.3	1.9	4.8	4,157,743	10	52	192	6	39.3	490	
16	Black Sea	2,453,129	187	84.4	4.6	11.0	2,224,991	31	91	176	24	89.3	198	81
17	Red Sea	935,189		23.4	30.9	45.7	134,100	10	14					
18	Baltic Sea	1,846,881	672	58.5	0.0	41.5	1,579,943	61	86	6	41	70.9	8	4
19	Hudson Bay	3,753,826	1549	46.7	8.1	45.3	2,875,305	33	77	2	5	6.5	30	8
	Oceania Islands	118,963	10										1148	9646
	Sum	120,604,352		69.7	8.8	21.5	95,655,063	2109	79	9542	908	63.7	16,403	

(*continued on next page*)

Table 2 (*continued*)

ID	Drainage Region	A_T	T_e	Seds.	Extr.	Endog.	A_b	N	A%	Q_b SS	N	Q SS%	Q_{AT} SS	Y SS
		km^2	Myr	%	%	%	km^2			Mt yr^{-1}			Mt yr^{-1}	t km^{-2} yr^{-1}
	Sum exorheic	110,095,498					91,497,321	2099	83	9349	902	66.9	15,914	
	Sum ex. w/ Oceania Isl.	110,214,461					91,616,284		83	10,497			17,061	
	T_{ew} (Myr)	445					449			312			313	
	%Seds	68.8					68.8			69.2			66.0	
	%Extr.	9.4					9.1			11.4			14.1	
	%Endog.	21.8					21.9			19.4			20.0	

ID	D	Q_b	N	Q%	Q_{AT}	R	c Sr_d	$^{87}Sr/^{86}Sr_w$	A_b Sr	% total	Q_b	% total	N	Q_S Sr
	m Myr^{-1}	km^3 yr^{-1}			km^3 yr^{-1}	cm yr^{-1}	μg l^{-1}		km^2	%	km^3 yr^{-1}	%		kg yr^{-1} $k-m^2$
1	3	2606	39	89	2934	22	82	0.7096	6,470,993	55	1511	52	6	19
2	57	685	40	81	843	23	159	0.7116	2,037,373	67	400	47	23	31
3	34	2430	151	85	2852	31	118	0.7140	5,992,860	74	1400	49	26	28
4	20	690	253	79	874	44	408	0.7093	697,229	42	181	21	11	106
5	42	9782	117	89	11,024	67	28	0.7125	11,046,697	75	8486	77	10	22
6	13	2140	76	85	2508	22	15	0.7175	6,770,000	66	1484	59	3	3
7	34	429	75	81	527	9	163	0.7123	2,179,597	43	117	22	6	8
8	185	2897	103	62	4731	49	100	0.7152	4,348,328	68	2174	47	23	52
9	101	5196	221	69	7494	53	186	0.7104	4,511,076	43	2199	29	19	91
10	73	1336	151	75	2154	40	115	0.7086	2,706,877	65	837	47	11	40
11	408	715	87	52	1379	113	47	0.7055	109,881	15	150	11	9	64
12	50	418	145	66	635	14	123	0.7122	1,198,383	31	78	12	16	8
13														
14	54	442	128	71	622	11	357	0.7077	3,099,000	72	140	22	2	16
15		524	9	52	1016	13		0.7082	0	0	0	0	2	
16	32	392	25	90	435	18	235	0.7088	1,791,720	81	291	67	4	38
17														
18	2	435	68	81	535	29	115	0.7120	1197,279	76	358	67	40	34
19	3	638	29	76	845	22	29	0.7172	2,552,499	89	539	64	16	6
	3859	250			250		200	0.7045	118,963		250			
		31,769	1702	76	41,409	33								
		31,245	1693	79	40,392	37	103		56,709,788	54	20,345	51	227	29
		31,495			40,642		104	0.71106	56,828,751		20,595			
		397			387				468		415			
		67.8			67.5				68.5		67.3			
		10.6			11.4				8.7		9.7			
		21.5			21.3				22.6		22.3			

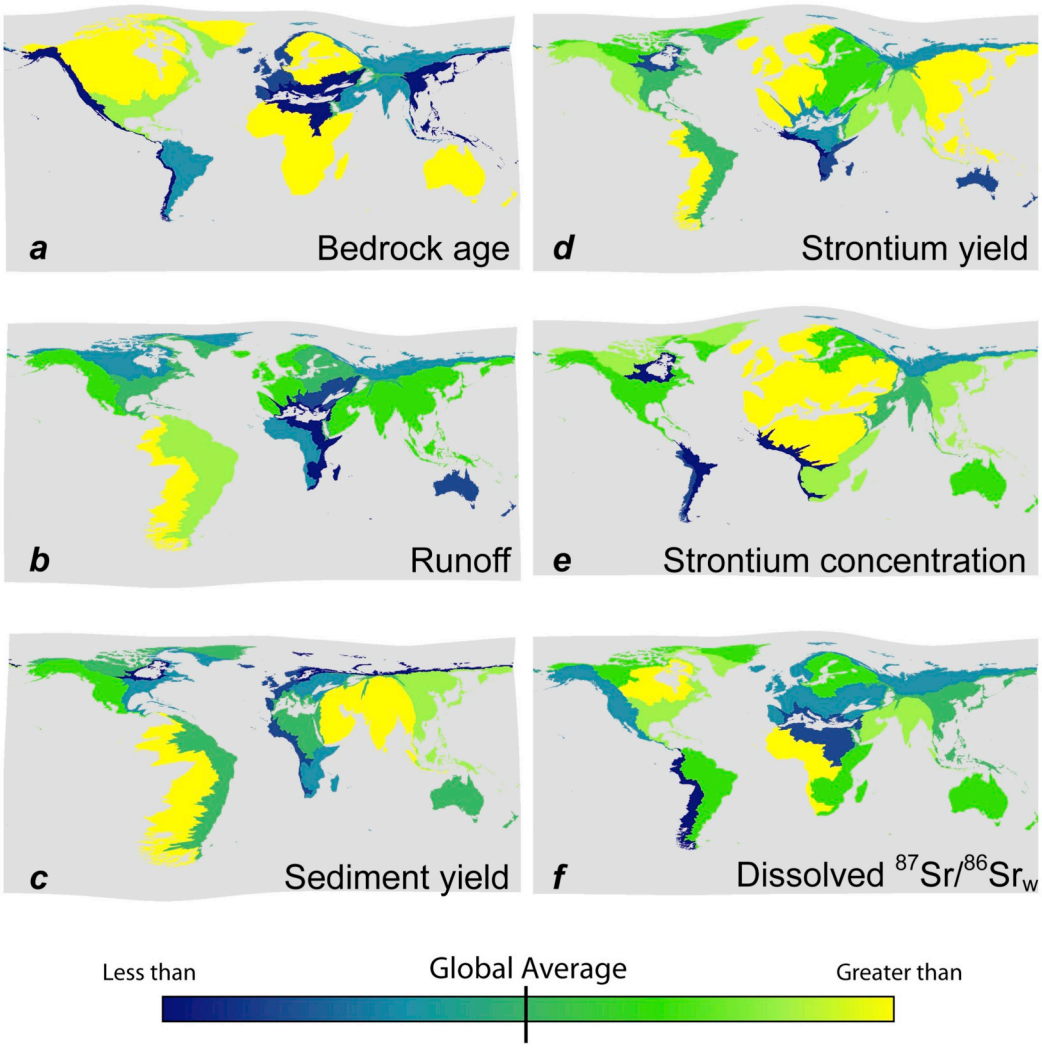

Fig. 10. Cartograms of large-scale drainage regions with average annual values of a) bedrock age (Myr) with a minimum value of 96 (dark blue: Western South America), a global average of 445, and a maximum value of 1549 (yellow: Hudson Bay); b) runoff (mm yr^{-1}); c) sediment yield (t yr^{-1} km^{-2}), with a minimum value of 4 (dark blue: Baltic Sea), a global average of 155, and a maximum value of 1019 (yellow, Western South America); d) strontium yield (kg Sr yr^{-1} km^{-2}), with a minimum value of 3 (dark blue: Western Africa), a global average of 29, and a maximum value of 106 (yellow: Western Europe); e) strontium concentration (μg L^{-1}), with a minimum value of 15 (dark blue: Western Africa), a global average of 104, and a maximum value of 408 (yellow: Western Europe); f) dissolved $^{87}Sr/^{86}Sr$, with a minimum value of 0.7055 (dark blue: Western South America), a global average of 0.7105, and a maximum value of 0.7175 (yellow: Western Africa).

4.2. Dissolution of land-derived particulate matter

As the vast majority of the riverine Sr flux is carried in dissolved form (Martin and Meybeck, 1979), contributions from the particulate riverine load are usually neglected in the mass balance of the dissolved load. However, in locations where reactive continental material – such as young basaltic suspended matter – is transported quickly into the marine environment where it continues to react, the continental Sr flux to seawater could involve the suspended load. This flux is temporally decoupled from current riverine fluxes. Jones et al. (2012) provide experimental evidence for continuing dissolution of land-derived particulate matter in seawater. Their laboratory batch experiments show dissolution of up to 27% of the Sr contained in riverine suspended particulate matter over a period of 6 months in seawater, the maximum duration investigated. As riverine particulate matter of volcanic origin, particularly volcanic ash, is generally more reactive than suspended matter of average crustal composition, this flux could add to the flux of unradiogenic Sr of continental pedigree to seawater. Jones et al. (2012) estimate that (1.3 to 3.2) × 10^{11} g yr^{-1} of Sr is added to seawater from this source. This estimate, however, is based on the assumption that 45% of the global riverine detrital load is volcanically derived, a value that is likely 2–3 times too high given our understanding of the chemical composition of riverine and marine sediments (Goldstein, 1988; Plank and Langmuir, 1998). A global Sr flux from this source of < 10^{11} g yr^{-1} (~10^{9} mol yr^{-1}) with a yet to be determined average $^{87}Sr/^{86}Sr$ (possibly ~ 0.705) appears more realistic. Jones et al. (2012) also estimate that dissolution of volcanic ash deposited directly on the ocean adds at most (1 to 2) × 10^{9} g yr^{-1} ([1.1 to 2.3] × 10^{7} mol yr^{-1}) of presumably mostly unradiogenic Sr (~0.705) to seawater.

4.3. Attempt at a steady-state mass balance

At present (Table 3), the combined sources of dissolved riverine Sr, Sr in SGD, and Sr released from land-derived particulate matter to seawater deliver between 5.5 × 10^{10} mol yr^{-1} of Sr with an average $^{87}Sr/^{86}Sr$ of 0.7108 and 7.7 × 10^{10} mol yr^{-1} of Sr with an average $^{87}Sr/^{86}Sr$ of 0.7103 to seawater. Adding contributions from submarine diffusive diagenetic fluxes, properly weighted according to carbonate (~5 × 10^{9} mol yr^{-1}, 0.7087) and non-carbonate (~5 × 10^{8} mol yr^{-1}, 0.7064) fluxes (Elderfield and Gieskes, 1982) to the sum of non-hydrothermal Sr contributions to seawater requires balancing between 6.1 × 10^{10} mol yr^{-1} of Sr with a $^{87}Sr/^{86}Sr$ of 0.71049 and

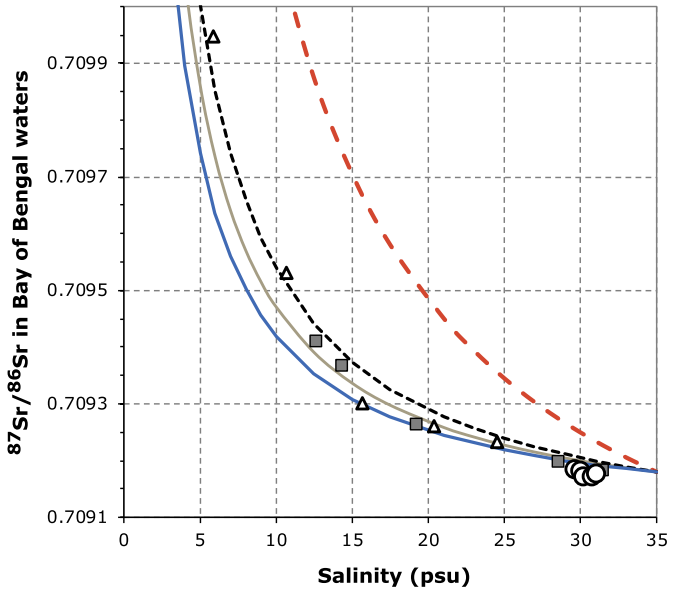

Fig. 11. Dissolved $^{87}Sr/^{86}Sr$ very versus salinity in the northern Bay of Bengal (white triangles: Shahbazpur River; gray squares: Sandwip Channel; white circles: northern Bay of Bengal; data from Beck et al., 2013). Plotted for comparison are mixing trends as inferred by Basu et al. (2001); red dashed line: average pure groundwater contribution; black stippled line: average mixture of groundwater and G-B river water ("Total Flux" in Basu et al., 2001, Table 2); brown solid line: Monsoon G-B river water; blue solid line: average G-B river water.

8.2×10^{10} mol yr^{-1} of Sr with a $^{87}Sr/^{86}Sr$ of 0.71008 with submarine hydrothermal contributions in order to achieve steady state for the modern ocean with a $^{87}Sr/^{86}Sr$ of 0.70918. The required unradiogenic (0.7037) flux of Sr is ~1.4×10^{10} mol yr^{-1}. This estimate exceeds most previous estimates of the submarine hydrothermal Sr fluxes from combined high- and low-temperature vent fluids (e.g.; Palmer and Edmond, 1989; Bickle and Teagle, 1992; Elderfield and Schultz, 1996; Davis et al., 2003; Coogan and Dosso, 2012). Even if contributions from ridge flank hydrothermal Sr fluxes are considered (Butterfield et al., 2001; Nielsen et al., 2006), Davis et al. (2003) argue that available data on ridge and ridge-flank ocean crust alteration limit the total unradiogenic Sr flux to seawater to at most 40% of what is required to balance the Sr budget of modern seawater. The resulting non-steady state model of modern seawater $^{87}Sr/^{86}Sr$ is consistent with the $^{88}Sr/^{86}Sr$ composition of seawater and our current understanding of its major sources and sinks (e.g. Krabbenhöft et al., 2010; Pearce et al., 2015).

5. A terrestrial perspective of the seawater $^{87}Sr/^{86}Sr$ record

Spatial variations in the $^{87}Sr/^{86}Sr$ of modern rivers significantly exceed the range of variations in $^{87}Sr/^{86}Sr$ of Phanerozoic and Neoproterozoic seawater (Figs. 1 and 3). Yet temporal variations in the $^{87}Sr/^{86}Sr$ of the continental endmember in multi-component mixing models of the marine $^{87}Sr/^{86}Sr$ record have not been quantitatively explored since Brass (1976), Palmer and Elderfield (1985, for the past 75 Myr), and Kump (1989, for the Phanerozoic). Instead, most multi-component models have focused on the balance between less radiogenic submarine hydrothermal sources of Sr and more radiogenic continental sources of Sr to seawater, with or without considering additional fluxes of other, less important, end-members (e.g. Spooner, 1976; Chaudhuri and Clauer, 1986; Davis et al., 2003; Hansen and Wallmann, 2003; Jones et al., 2012). Unfortunately, submarine hydrothermal fluxes of Sr to seawater are very difficult to reconstruct for the geologic past, one of the major challenges in paleoceanography. Using estimates of oceanic crust productions rates through time to quantify hydrothermal fluxes requires estimating the relative importance of ridge crest vs. ridge flank contributions to heat and fluid flows (Veizer, 1989; Veizer et al., 1999; Butterfield et al., 2001; Davis et al., 2003) and, ultimately, Sr fluxes. While attempts have been made to constrain such fluxes for the present (Bach and Humphris, 1999; Davis et al., 2003), extending such analyses into the geologic past quickly leads to deteriorating accuracy and precision due to the increasingly sparse and non-unique records of past ocean crust production rates (Rowley, 2002; Cogné and Humler, 2004, 2006; Van Der Meer et al., 2014). In our conceptual model we therefore hold submarine hydrothermal Sr fluxes and $^{87}Sr/^{86}Sr$ constant at present-day values.

For this conceptual model we use the relationship between bedrock age and dissolved $^{87}Sr/^{86}Sr$ to invert the non-hydrothermal component of the marine $^{87}Sr/^{86}Sr$ record for the age of the continental bedrock that contributed Sr to the ocean in the geologic past. This age has to be viewed as the Sr-flux-weighted average bedrock age of the exorheic

Table 3
Minimum and maximum strontium estimates of Sr flux (in billion moles per year) as well as $^{87}Sr/^{86}Sr$ for global rivers (weighted according to Sr flux and corrected for regional biases, see text for details), including smaller ocean islands of Oceania, submarine groundwater discharge (SGD) according to Beck et al. (2013), dissolution of riverine sediment in seawater (Jones et al., 2012), and dissolution of volcanic ash deposited on the ocean (Jones et al., 2012). Diffusive diagenetic contributions to Sr in seawater have been recalculated based on Elderfield and Gieskes (1982). Minimum and maximum flux and isotope ratio estimates for all non-hydrothermal contributions are abbreviated as "Non-hydrothermal". Minimum, maximum and our preferred estimate of Sr fluxes and isotope ratios of submarine hydrothermal sources needed to balance the present day seawater budget are also given, as is the present-day $^{87}Sr/^{86}Sr$ of seawater.

	Strontium flux		$^{87}Sr/^{86}Sr$	
	Minimum	Maximum	Minimum	Maximum
	10^9 mol yr^{-1}			
Global rivers	47.6		0.71107	
SGD	7	28	0.7089	
Rivers + SGD	54.6	75.6	0.71027	0.71079
Sediment dissolution	1		0.705	
Volcanic ash dissolution	0.0114	0.0228	0.705	
All continental sources	55.6	76.6	0.71020	0.71069
Diagenetic + diffusive sources	5.5		0.70849	
All non-hydrothermal sources	61.1	82.1	0.71008	0.71049
Hydrothermal contributions needed for steady-state seawater budget				
	11.1	12.0	0.7025	
	13.0	14.1	0.7035	
	13.5	14.6		0.7037
Modern seawater			0.70918	

portion of the continents, including ocean islands. To avoid confusion, we emphasize that this new parameter is not simply the average bedrock age of the continental bedrock at any given time in the geologic past. Rather, it is an element-specific, flux-weighted exorheic bedrock age that is different for each radiogenic isotope system. This model expands the approach Palmer and Elderfield (1985) and Kump (1989) took in estimating changes in riverine dissolved $^{87}Sr/^{86}Sr$ that are needed to explain observed variations in seawater with all other source and sink terms held constant. Kump (1989) concluded that "changes in stream isotopic composition, reflecting increasing and decreasing contributions from shield regions of the continents to the global riverine Sr flux, appear to present the most consistent explanation for long-term secular change in the $^{87}Sr/^{86}Sr$ of seawater."

The present-day slope of the global correlation of best average dissolved $^{87}Sr/^{86}Sr$ vs. bedrock age ($[2.15 \pm 0.20]\ 10^{-5}$; based on Reed, 1992, 2010) that is defined by large scale drainage regions is consistent with an effective $^{87}Rb/^{86}Sr$ of ~1.5. This value can be interpreted as the Sr-flux-weighted effective $^{87}Rb/^{86}Sr$ of the continental crust that delivers Sr to seawater. The value is similar to reasonable estimates for the upper crust, and 2–3 times higher than the $^{87}Rb/^{86}Sr$ of bulk continental crust (Goldstein, 1988; Hofmann, 1988; McLennan, 2001). The slope of this global correlation has likely not changed systematically since the Neoproterozoic. This is because its less radiogenic end is anchored at the very slowly changing (i.e. $^{87}Rb/^{86}Sr < 0.1$) $^{87}Sr/^{86}Sr$ value for mantle-derived rocks, whereas the position of the old radiogenic endmember is balanced by the time-integrated growth of ^{87}Sr that tends to steepen the slope and the increasing age range through geologic time that tends to decrease the slope. We therefore argue that the modern slope estimate can be used to invert the $^{87}Sr/^{86}Sr$ record of seawater in an attempt to reconstruct changes in the T_{bexSr} – the effective bedrock age of the exorheic land surface weighted according to the dissolved Sr flux.

The observed temporal variations in the $^{87}Sr/^{86}Sr$ of seawater require variations in global bedrock age between ~190^{+20}_{-15} and 335^{+35}_{-30} Myr for the entire Phanerozoic and between ~260^{+70}_{-40} and 330^{+35}_{-30} Myr for the past 30 Myr (Fig. 12a). These are maximum age ranges because processes that expose older bedrock also tend to enhance erosion rates and thus the flux of Sr to seawater. In this interpretation, the period from ~520 Ma to ~150 Ma is characterized by a progressive rejuvenation of global bedrock that was proceeded and followed by periods of progressive aging from 800 Ma to ~520 Ma and since ~150 Ma, respectively. Interestingly, the inferred rejuvenation is

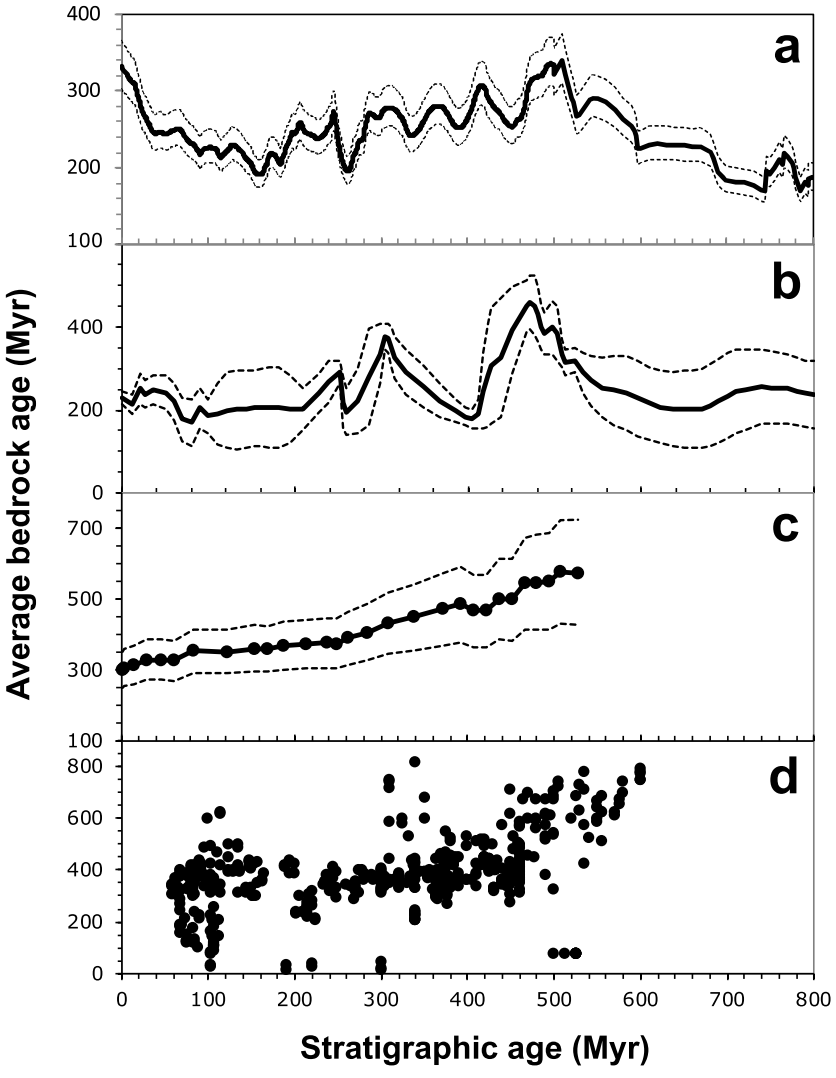

Fig. 12. a) Average global bedrock age required for generating a sufficiently radiogenic global riverine $^{87}Sr/^{86}Sr$ to account for the measured $^{87}Sr/^{86}Sr$ of seawater assuming constancy in the ratio of hydrothermal versus continental inputs throughout the Phanerozoic. The ratio of hydrothermal to continental inputs is held constant based on present-day values for hydrothermal (0.7035, Bach and Humphris, 1999), continental (0.7107, this review) and seawater (0.709169, McArthur et al., 2001) components. The calculation also assumes that the ratio of global bedrock age weighted according to bedrock area (presently 445 Myr for the sum of 16 out of 19 Graham regions) to the average age weighted according to Sr flux (presently 331 Myr) has remained constant; b) Neodymium isotope record of seawater (values from Keto and Jacobsen, 1988, stippled lines are based on upper and lower Nd isotope estimates) inverted for globally averaged bedrock age according to the present-day correlation between the Nd isotope composition of continental runoff, averaged for large-scale drainage regions, and average bedrock ages of such regions; c) Average bedrock ages for the paleogeologic reconstructions by Ronov and coworkers (Ronov, 1989, 1993). Bedrock ages are calculated by partitioning the area abundances of Ronov's lithologic units (values from Bluth and Kump, 1991, Table 4) for each time interval into three lithotypes (sedimentary rocks, extrusive volcanic rocks, endogenous rocks) for which global bedrock ages have been determined (Peucker-Ehrenbrink and Miller, 2007b). Bedrock ages of the lithotypes are based on an exponential age model rather than geometric means of upper and lower limits of rectangular age distributions. This yields averages of 201 Myr for sedimentary rocks, 283 Myr for extrusive volcanic rocks, and 1375 Myr for endogenous rocks. For endogenous bedrock (y) we adjusts the average age for each time period by subtracting the stratigraphic age of that period (x) from the present-day average endogenous bedrock age, i.e., $y = 1375 - x$ (Myr). In contrast, we keep the bedrock ages of sedimentary rocks and extrusive volcanic rocks unchanged, thus allowing for formation and recycling of the latter two lithologic units, but not the endogenous bedrock. Without this correction the average bedrock age of the Earth's surface were ~250 Myr older in the early Phanerozoic when the correction is largest; d) Average bedrock ages based on Nd isotope values of North American clastic sediments (Andersen and Samson, 1995; Bock et al., 1996; Boghossian et al., 1996; Dickinson et al., 2003; Garzione et al., 1997; Gleason et al., 1994, 1995; Patchett and Gehrels, 1998; Patchett and Gehrels, 1998; Patchett et al., 1999a, 1999b, 2004; Ross et al., 2005), inverted using the present-day relationship between clastic sediments derived from large-scale drainage regions and average bedrock ages of such regions (Peucker-Ehrenbrink et al., 2010). Some data points with negative bedrock ages and a few data points with ages exceeding 900 Myr are not shown.

consistent with the apparent decrease in exposed Precambrian shield area during the Paleozoic and early Mesozoic (Ronov, 1989; Bluth and Kump, 1991). The most recent aging trend is likely caused by exposure of older bedrock due to the combined effects of orogeneses and glaciations.

The first-order feature of an asymmetric trough is decorated with second-order (< 50 Myr) fluctuations. Periods of rapid apparent rejuvenation of continental drainage may represent rapid steepening of regional age-$^{87}Sr/^{86}Sr$ slopes during regional metamorphism, or cannibalistic recycling of older sediments during mountain building; both processes lead to younger bedrock ages. Periods of rapid apparent aging of continental bedrock can be caused by regional uplift, associated removal of young sediments and exposure of older bedrock, or by amagmatic crustal extension and exposure of lower crustal metamorphic rocks in core complexes (Buck, 1991). Alternatively, apparent bedrock aging may reflect glacial denudation of shield cover and exposure of Precambrian shields (Armstrong, 1971). Changes in the submarine release of unradiogenic Sr at spreading ridges or during the emplacement of large igneous provinces may have contributed to second- and third-order variations (see Figs. 1 and 2). For instance, Kent and Muttoni (2008) argue that the northward movement of the Indian subcontinent after the eruption of the Deccan Traps transited the humid tropics during the Eocene and early Oligocene, thereby contributing to enhanced supply of less radiogenic Sr to the oceans. Several deviations to younger bedrock ages (that is, less radiogenic Sr) that are linked to inflections in the $^{87}Sr/^{86}Sr$ record appear to be correlated mostly with subaerial, rather than submarine, volcanic eruptions that have changed continental drainage lithology (McArthur et al., 2001). Temporal trends in T_{bexSr} can also be caused by paleogeographic reorganization, changes in total land area and related changes in regional or global hydrology. For example, very little dissolved Sr currently reaches the ocean from the relatively old bedrock exposed in Australia. Most importantly, it seems overly simplistic to link increasing $^{87}Sr/^{86}Sr$ values of seawater to increases in the continental flux of Sr, or – by extension – to more intense continental weathering.

6. Supporting evidence

The validity of the proposed record of paleo-bedrock ages can be compared to at least three independent records of continental evolution: the neodymium isotope composition of seawater (Keto and Jacobsen, 1988), the evolution of detrital source areas on the North American continent (e.g. Patchett et al., 1999a, 1999b), and global paleogeologic reconstructions (Ronov, 1989; Bluth and Kump, 1991; Cao et al., 2017).

6.1. The neodymium isotope record of seawater

Few attempts have been made to estimate regionally or globally averaged ε_{Nd} of paleo-seawater, and results are uncertain owing to the scarcity of data and knowledge of the paleogeography of ocean basins (e.g., Hooker et al., 1981; Keto and Jacobsen, 1988). Keto and Jacobsen (1988) propose a record of globally averaged Nd isotope composition of seawater for the past 800 Myr. This record is based on only ~80 Nd isotope analyses. Data density is quite high for the past 100 Myr, but very low (6) for the period 600–800 Ma, leading to variable confidence with which the record is known. Since this pioneering study no further attempt has been made to update this pioneering reconstruction with the wealth of new Nd isotope data for modern (van der Flierdt et al., 2016) and paleo-seawater. A new attempt at a global integration would provide a valuable perspective of continental weathering processes, because neodymium in seawater is almost exclusively of continental origin (Michard et al., 1983; Tachikawa et al., 2003; Peucker-Ehrenbrink et al., 2010).

The Phanerozoic marine ε_{Nd} record (Keto and Jacobsen, 1988) can be inverted to bedrock ages of continental drainage using the global correlation of bedrock age with detrital ε_{Nd} (Fig. 4b in Peucker-Ehrenbrink et al., 2010). For this inversion the Phanerozoic marine ε_{Nd} record is corrected from the original Van Eysinga (1975) timescale to the GTS2012 timescale (Gradstein et al., 2012). Then, the ε_{Nd} of paleoseawater is inverted to bedrock age of the continental detrital source (T_{bd}, in million years [Myr]) using the linear correlation that has been established with present-day isotope values, $T_{bd} = [-24 \pm 6]\varepsilon_{Nd} + [83 \pm 64]$, ($r^2 = 0.65$), using data from Peucker-Ehrenbrink et al. (2010) and the linear least square fit of Reed (1992, 2010) with uncertainties in both parameters.

In order to compare the record of paleo-seawater ε_{Nd} that is based on age-corrected isotope values ($\varepsilon_{Nd}[T]$ of Keto and Jacobsen, 1988) with modern data ($\varepsilon_{Nd}[0]$), we assume – as we did for the correlation between the riverine $^{87}Sr/^{86}Sr$ composition and bedrock ages – that the slope of the global correlation has not significantly changed over time.

We argue that this inversion yields the mean bedrock age of the continental drainage that contributes detrital – and by inference dissolved – Nd to seawater (Fig. 12b). The results therefore do not have to agree with those derived from dissolved $^{87}Sr/^{86}Sr$ that are influenced by different lithologies and processes. The Nd-based paleorecord shows a first order increase in the mean bedrock age from ~240 Myr at 800 Ma to ~450 Myr at ~470 Ma. This increase is followed by a general rejuvenation of global bedrock to ~200 Myr in the Jurassic to early Cretaceous. Since then, T_{bd} seems to have increased again slightly to a present-day value of ~230 Myr. This value is slightly younger than the mean bedrock age of 313 Myr of drainage areas that presently contribute to the detrital Nd load to the oceans. Large but poorly documented oscillations in T_{bd} with periods of 50–100 Myr indicate that second-order processes affect the composition of the continental drainage that govern to the delivery of detrital Nd to seawater. The observed variations in T_{bd} are equivalent to changing proportions in the exposure and erosion of old endogenous relative to young volcanic and sedimentary bedrock.

6.2. Phanerozoic paleogeologic reconstructions

The seawater Sr and Nd isotope evidence can be compared with the only attempt at reconstructing lithologic maps of the global continental surface throughout the Phanerozoic (Ronov, 1989, and references therein; Bluth and Kump, 1991). This record is of low temporal resolution and thus does not show fluctuations on time scales < 30 Myr. Events such as the emplacement of large igneous provinces (Figs. 1 and 2) that can affect the marine Sr isotope record are therefore not registered immediately in this record. Bluth and Kump (1991, Table 4) have quantitatively evaluated paleogeologic maps (Ronov, 1989) in an attempt to assess changes in bedrock lithology during the Phanerozoic. In order to invert this record of paleogeology to bedrock age it is necessary to combine Ronov's (1989) six sedimentary subunits – coal, shale, evaporite, chert, sandstone and carbonate – into a single sedimentary bedrock unit for which global bedrock age data exist. Paleo-reconstructions of bedrock areas covered by “volcanic rocks” and “shield rocks” (Ronov, 1989; Bluth and Kump, 1991) can be compared to respective digital data on “volcanic bedrock” and “endogenous (igneous and metamorphic) bedrock” that are delineated in the global GIS-based bedrock map (Commission for the Geologic Map of the World, 2000; Peucker-Ehrenbrink and Miller, 2007b). In the future, this analysis could be refined by combining global stratigraphic maps used in this study with the Global Lithologic Map (GliM; Hartman and Moosdorf, 2012). In contrast to endogenous bedrock (1375 ± 185 Myr, 1σ, exponential age model), sedimentary (201 ± 38 Myr, 1σ) and volcanic bedrock (283 ± 48 Myr, 1σ) have young mean ages that reflect their formation near the Earth's surface (Wilkinson et al., 2009) where erosion and cannibalistic recycling cause rapid turnover. The relative spatial abundances of sedimentary, extrusive, and endogenous bedrock together with their mean bedrock ages are used to compute the mean age of continental bedrock for each time point (stratigraphic age) of

Ronov's paleo-reconstruction (Fig. 12c). These simplifications allow inverting temporal variations in the relative abundance of bedrock lithologies to bedrock ages. The good agreement between the first-order features of the paleogeology and the $^{87}Sr/^{86}Sr$ inversions (Fig. 12) instills confidence in the general validity of paleogeologic reconstructions for the Phanerozoic (Ronov, 1989; Bluth and Kump, 1991; Gibbs et al., 1999).

The nearly monotonous increase in the inferred mean bedrock age of the continental crust from ~300 Myr at present to ~575 Myr in the early Phanerozoic mainly reflects the greater abundance of "shield rocks" in the paleolithologic reconstructions (Ronov, 1989; Bluth and Kump, 1991). As discussed by Bluth and Kump (1991), this greater abundance may reflect the dearth of deposition in the interiors of South America and Africa during the Paleozoic. Consequently, those continental interiors are delineated as "pre-Riphean" shield exposure on the paleolitholigic maps of the Paleozoic. Intensification of deposition throughout the Mesozoic and Cenozoic led to progressive loss of shield exposure. However, Bluth and Kump (1991) could not rule out the possibility that the greater exposure of pre-Riphean shields in the Paleozoic results from a procedural artefact in the computation of lithologic abundances, because "shield rock" is the assumed lithology once all overburden has been stripped. In addition, shield cover that once existed but had subsequently been eroded cannot be reconstructed with their procedure. It is thus likely that some of the "shield rock" delineated in their maps was instead covered by Phanerozoic volcanic or sedimentary sequences. However, the interpretation that some fraction of the greater exposure of shield rocks in the Paleozoic is real finds support in the global Nd isotope evolution of seawater and the record of detrital sediment sources on the North American continent.

Interestingly, Cao et al. (2017, their Fig. 4) in their reconstruction of globally integrated continental arcs lengths found a trend towards increasing arc length starting ~300–350 Ma. A trend towards shorter global arc lengths started between 70 Ma and 100 Ma and continues into the present. The broad peak in global arc length generally correlates with the abundance of global detrital zircon ages that peak in abundance between ~70–170 Ma. Today, continental arcs are significant sources of unradiogenic Sr to seawater (Fiege et al., 2009). We posit that the coincidence between continental arc length, our inferred younger bedrock ages for the continental drainage that delivers Sr to the ocean, and the less radiogenic composition of seawater strontium create a coherent picture of continental drainage evolution in the Phanerozoic.

6.3. Temporal changes in the continental source areas of detrital matter

The Nd isotope compositions of detrital sediments from North American provide an independent, though regional, estimate of the composition and age structure of the respective source regions of detrital matter over time (e.g., Patchett et al., 1999a). Source areas of detrital matter to the oceans do not have to coincide with those of dissolved inputs to seawater. Therefore, direct comparison of geochemical information extracted from detrital archives with proxies for dissolved inputs is fraught with ambiguity. The above mentioned 74 million offset in bedrock ages between areas delivering detrital vs. dissolved material to the ocean is just one example of this bias. The realization that records of dissolved and detrital inputs to the oceans do not need to correspond led Berner and coworkers to abandon the GEOCARB II parameterization of weathering intensity – or more precisely the weathering-uplift factor $f_R(t)$ – by means of the marine $^{87}Sr/^{86}Sr$ record in favor of a direct measure of detrital inputs to the oceans (Wold and Hay, 1990; Ronov, 1993) in the GEOCARB III model (Berner and Kothavala, 2001). This sentiment was recently reiterated in a comparison of the seawater $^{87}Sr/^{86}Sr$ record with a Phanerozoic compilation of Hf isotope compositions of detrital zircons that concludes that the marine $^{87}Sr/^{86}Sr$ record is not a good proxy for continental weathering intensity (Bataille et al., 2017). Fig. 12d displays bedrock ages based on 537 Nd isotope analyses of detrital sediments from North America (DePaolo, 1981; Patchett and Gehrels, 1998; Patchett et al., 1999a, 2004; Gleason et al., 1994, 1995; Boghossian et al., 1996; Garzione et al., 1997; Bock et al., 1996; Andersen and Samson, 1995; Dickinson et al., 2003; Ross et al., 2005). The Nd isotope compositions of suspended matter in the Fraser River in conjunction with the respective bedrock ages of the Fraser River and its tributary drainage basins allow us to relate Nd model ages of modern river suspended loads to the bedrock age of their drainage basins. This relationship can be used to invert the record of sediment Nd model ages from North America to calculate bedrock ages of the respective drainage regions as shown in Fig. 12d. The record shows a trend towards younger model ages of detrital sediments during the Paleozoic followed by constant values during the Mesozoic. Values for the last 100 Myr scatter considerably due to incomplete homogenization of the young detritus that is mainly derived from the still evolving Cordilleran source (Patchett et al., 1999a). We emphasize that this record is not yet global, though such an attempt seems warranted. A complementory worldwide record of Hf model ages using U-Pb-dated zircons is broadly consistent with this interpretation, provided that the increasing contribution of new crust relative to the existing continental crust from ~500 Ma to ~200 Ma that was followed by a reversal during the last 200 Ma (Dhuime et al., 2012, Fig. 2A) resulted in increased surface exposure of young crust during the Paleozoic and early Mesozoic.

7. Conclusions and perspectives

The seawater $^{87}Sr/^{86}Sr$ record reflects the combined effects of the yet to be quantified history of the submarine hydrothermal Sr flux to seawater and the evolution of continental drainage biased towards Sr-rich, easily weatherable lithologies such as limestone. Despite this bias the seawater $^{87}Sr/^{86}Sr$ record is currently the best available radiogenic marine isotope record for making inferences about the changing lithologic composition and bedrock age structure of the continental drainage. The $^{187}Os/^{188}Os$ record of seawater has not been reconstructed for most of the Phanerozoic, but may eventually yield insights into the exposure of osmium-rich lithologies such as ultramafic rocks and sedimentary rocks rich in organic matter (Peucker-Ehrenbrink and Ravizza, 2001, 2012). Seawater is heterogenous with respect to neodymium, hafnium and lead isotopes. Their seawater records therefore require regional averaging before globally relevant information can be extracted. An attempt to reconstruct the globally averaged Nd isotope record of seawater is suggestive of a transition from no crustal growth to net crustal growth about 450 Myr ago (Keto and Jacobsen, 1988), consistent with Phanerozoic rejuvenation of continental bedrock. A new attempt aimed at incorporating the wealth of new Nd isotope data for seawater that are now available should be made to update the 30 year old assessment of Keto and Jacobsen (1988). Combined, these radiogenic marine isotope records will provide new insights into past bedrock geology of the continental drainage that are needed for models of past ocean and atmospheric chemistry.

The most important unresolved issue that affects further refinements of the modern riverine Sr budget is the claim by Rahaman et al. (2011) that the $^{87}Sr/^{86}Sr$ of the Ganges River has increased over the past 5 kyr from ~0.715 to the present values of 0.73–0.74, a significant change that is not seen in the geochemistry of the suspended particulate load of the river (Galy et al., 2010). If the soil carbonates from the Gangetic floodplain that Rahaman et al. (2011) analyzed faithfully represent the isotope composition of the Ganges River, and assuming the Sr flux of the Ganges River has not changed, the change in $^{87}Sr/^{86}Sr$ would have caused a recent increase in the $^{87}Sr/^{86}Sr$ of the drainage region Arabia-India-SE Asia from 0.7140 to 0.7152, and the global riverine $^{87}Sr/^{86}Sr$ by 0.00014 units (from 0.71093 to 0.71106).

With the exception of tributaries to the Fraser and Mississippi rivers, the wealth of data from smaller rivers and streams that do not drain directly into the ocean has not been utilized for this review. Examples of such datasets are the detailed studies of the hydrochemistry of the

Amazon (Allègre et al., 1996; Santos et al., 2015), Orinoco (Edmond et al., 1995, 1996; Stallard and Edmond, 1983), several of the large Russian Arctic rivers (Huh et al., 1998; Huh and Edmond, 1999; Mavromatis et al., 2016), Rhine (Buhl et al., 1991), Danube (Pavellek et al., 2002), Connecticut (Douglas et al., 2002), Garonne (Semhi et al., 2000), Orange (de Villiers et al., 2000), Ganges (Galy et al., 1999; Bickle et al., 2005; Tripathy et al., 2010), Congo (Negrel and Dupre, 1993; Allègre et al., 1996) and Yangtze (Noh et al., 2009; Luo et al., 2014) rivers. However, such data has been used at the regional scale to calibrate models of the isotopic composition of runoff that are based on bedrock lithology for the conterminous United States of America (Bataille and Bowen, 2012) and Alaska (Bataille et al., 2014).

Technological advances, specifically laser ablation (LA) $^{87}Sr/^{86}Sr$ analysis by multi-collector inductively coupled plasma mass spectrometry (MC-ICPMS), have opened the door to a new source of riverine $^{87}Sr/^{86}Sr$ data from biominerals formed by aquatic organisms (fish otoliths, scales, spines, fin rays, freshwater bivalves; e.g. Pouilly et al., 2014; Willmes et al., 2016) that complement traditional isotope analyses on corresponding waters. Such LA-MC-ICPMS data has not been fully integrated into compilations of river biogeochemistry, in part because of the difficulty of establishing dissolved Sr concentrations from such measurements. However, LA-MC-ICPMS analyses make it possible to reconstruct paleo-$^{87}Sr/^{86}Sr$ of systems affected by anthropogenic modifications and river capture, and may help to reconstruct the temporal evolution of dissolved $^{87}Sr/^{86}Sr$ in, for instance, the Ganges River. Such data close the loop to some of the earliest assessments of the dissolved $^{87}Sr/^{86}Sr$ in natural waters that utilized biogenic minerals (Gast, 1955; Faure et al., 1967) to extract sufficient Sr for mass spectrometric analyses in an effort to overcome the laborious extraction of sufficient quantities of Sr from natural waters.

Further refinement of our understanding of continental contributions to the marine $^{87}Sr/^{86}Sr$ record, particularly for the present (e.g. Bataille et al., 2014) requires quantitative treatment of the distribution of rainfall (climate), soil properties (e.g., formation of regolith), propensity to generate dissolved Sr, as well as geomorphology. However, the accuracy and precision with which these additional parameters can be reconstructed for the geologic past decrease with increasing geologic age (e.g., Tardy et al., 1989; Gibbs et al., 1999; Donnadieu et al., 2006; Godderis et al., 2014). For instance, Tardy et al. (1989) estimate that continental runoff during the Phanerozoic has varied from 38,500 $km^3\,yr^{-1}$ (Lower Jurassic) to values as high as 63,460 $km^3\,yr^{-1}$ (Mid and Lower Cambrian), whereas Gibbs et al. (1999) constrain variations in continental discharge over the past 240 million years to 33,500–74,100 $km^3\,yr^{-1}$. Variations in global annual runoff by less than a factor of two is also consistent with results from the GEOCLIM model (Donnadieu et al., 2006) that returns low runoff values (23.5 cm yr^{-1}) for the Middle-Late Triassic and high values (42.4 cm yr^{-1}) for the Mid Cretaceous, findings that are consistent with those of Godderis et al. (2014). Given the present-day relationships between dissolved riverine Sr concentration and discharge (Fig. 5), a factor a two change in discharge would have caused a change in the Sr flux to the ocean by between a factor of 1.4 to 1.9, thus modulating the required change in bedrock age (T_{bexSr}) to account for the observed change in the $^{87}Sr/^{86}Sr$ of seawater. In spite of obvious simplifications, the focus on bedrock age has the advantage of being testable against paleo-reconstructions of bedrock lithology (Ronov, 1989; Bluth and Kump, 1991).

In his insightful review of the seawater $^{87}Sr/^{86}Sr$ record Jan Veizer (1989) summarized the challenge of interpreting this record that is influenced by "at least four variables […]; none of these […] tightly constrained at present and even less so in the geological past. With four fluctuating and counteracting unknowns, a unique solution requires prior quantification of the Phanerozoic variations for $n - 1$ variables, a task beyond our present capabilities." Despite progress in the intervening three decades, we are still not able to solve this intriguing puzzle, and likely will not be able to unless we develop reliable tracers for chemical mass transfer by submarine hydrothermal circulation in the geologic past.

Acknowledgements

We thank Timothy Horscroft for the invitation to review this topic and for his patience during the circuitous path to completion. Detailed reviews by Christopher Pearce and Clement Bataille helped us refine some arguments and improve the presentation. David Rowley kindly provided his numerical estimates of ocean crust production rates for the past 180 Myr. John McArthur gave us permission to use his LOWESS 3.0 fit to the marine Sr isotope data for the Phanerozoic, and Yves Godderis made model estimates of paleo-runoff available to us. Jonathan Patchett let us use his large database of sedimentary $^{143}Nd/^{144}Nd$ data and gave us access to unpublished manuscripts. We also thank Kristina Brown for allowing us to use average Sr data for 19 rivers draining the Canadian Arctic Archipelago. We are indebted to Patrick Seyler for digging out sampling dates for the Amazon River at Óbidos from the late 1990s, and to Jose Mauro S. Moura for the related discharge data. We would also like to thank Tom Gross at Esri for creating a tool for quickly and efficiently creating Density Equalizing Cartograms from standard vectorized GIS data files. The link to this tool is: https://www.arcgis.com/home/item.html?id=d348614c97264ae19b0311019a5f2276. Mark Miller provided some bedrock data for watersheds at the early stages of this project. BPE acknowledges financial support from NSR-EAR-0087697, EAR-0125873, EAR-1226818 and ICER-1639557, from a grant from The van Beuren Charitable Foundation, as well as from WHOI's Investment in Research and Development Fund.

Appendix A. Supplementary data

Supplementary data to this article can be found online at https://doi.org/10.1016/j.chemgeo.2019.01.017.

References

Albarède, F., Michard, A., Minster, J.F., Michard, G., 1981. $^{87}Sr/^{86}Sr$ ratios in hydrothermal waters and deposits from the East Pacific rise and 21°N. Earth Planet. Sci. Lett. 55, 229–236.

Albarède, F., Vitrac-Michard, A., Minster, J.F., Michard, G., 1980. Strontium isotopic composition in hydrothermal systems. Eos Trans. AGU 61 (46), 994–995.

Allègre, C.J., Dupré, B., Négrel, P., Gaillardet, J., 1996. Sr-Nd-Pb isotope systematics in Amazon and Congo River systems: Constraints about erosion processes. Chem. Geol. 131, 93–112.

Allègre, C.J., Louvat, P., Gaillardet, J., Meynadier, L., Rad, S., Capmas, F., 2010. The fundamental role of island arc weathering in the oceanic Sr isotope budget. Earth Planet. Sci. Lett. 292, 51–56.

Andersen, C.B., Samson, S.D., 1995. Temporal changes in Nd isotopic composition of sedimentary rocks in the Sevier and Taconic foreland basins: increasing influence of juvenile sources. Geology 23 (11), 983–986.

Armstrong, R.L., 1971. Glacial erosion and the variable composition of strontium in seawater. Nature Phys. Sci. 230, 132–133.

Bach, W., Humphris, S.E., 1999. Relationship between the Sr and O isotope composition of hydrothermal fluids and the spreading and magma-supply rates at oceanic spreading centers. Geology 27, 1067–1070.

Bamber, J., van der Broeke, M., Ettema, J., Lenaerts, J., Rignot, E., 2012. Recent large increases in freshwater fluxes from Greenland into the North Atlantic. Geophys. Res. Lett. 39, L19501. https://doi.org/10.1029/2012GL052552.

Basu, A.R., Jacobsen, S.B., Poreda, R.J., Dowling, C.B., Aggarwal, P.K., 2001. Large groundwater strontium flux to the oceans from the Bengal Basin and the marine strontium isotope record. Science 293, 1470–1473.

Basu, A.R., Jacobsen, S.B., Poreda, R.J., Dowling, C.B., Aggarwal, P.K., 2002. Reply to Harvey. Science 296, 1563A.

Bataille, C.P., Bowen, G.J., 2012. Mapping $^{87}Sr/^{86}Sr$ variations in bedrock and water for large scale provenance studies. Chem. Geol. 304-305, 39–52.

Bataille, C.P., Brennan, S.R., Hartmann, J., Moosdorf, N., Wooller, M.J., Bowen, G.J., 2014. A geostatistical framework for predicting variations in strontium concentrations and isotope ratios in Alaskan rivers. Chem. Geol. 389, 1–15.

Bataille, C.P., Willis, A., Yang, X., Liu, X.-M., 2017. Continental igneous rock composition: a major control of past global chemical weathering. Sci. Adv. 2017 (3), e1602183.

Beck, A.J., Charette, M.A., Cochran, J.K., Gonneea, M.E., Peucker-Ehrenbrink, B., 2013. Dissolved strontium in the subterranean estuary – Implications for the marine strontium isotope budget. Geochim. Cosmochim. Acta 117, 33–52. https://doi.org/

10.1016/j.gca.2013.03.021.
Berner, R.A., Kothavala, Z., 2001. GEOCARB III: a revised model of atmospheric CO_2 over Phanerozoic time. Am. J. Sci. 301, 182–204.
Bickle, M.R., Chapman, H.J., Bunbury, J., Harris, N.B.W., Fairchild, I.J., Ahmad, T., Pomiès, C., 2005. Relative contributions of silicate and carbonate rocks to riverine Sr fluxes in the headwaters of the Ganges. Geochim. Cosmochim. Acta 69 (9), 2221–2240.
Bickle, M.R., Teagle, D.A.H., 1992. Strontium alteration in the Troodos ophiolite: implications for fluid fluxes and geochemical transport in mid-ocean ridge hydrothermal systems. Earth Planet. Sci. Lett. 113, 219–237.
Blum, J.D., Erel, Y., 1995. A silicate weathering mechanism linking increases in marine $^{87}Sr/^{86}Sr$ with global glaciation. Nature 373, 415–418.
Bluth, G.J.S., Kump, L.R., 1991. Phanerozoic paleogeology. Am. J. Sci. 291, 284–308.
Bock, B., McLennan, S.M., Hanson, G.N., 1996. The Taconian orogeny in southern New England: Nd-isotope evidence against addition of juvenile components. Can. J. Earth Sci. 33 (12), 1612–1627.
Boghossian, N.D., Patchett, P.J., Ross, G.M., Gehrels, G.E., 1996. Nd isotopes and the source of sediments in the miogeocline of the Canadian cordillera. J. Geol. 104 (3), 259–277.
Brass, G.W., 1976. The variation of the marine $^{87}Sr/^{86}Sr$ ratio during Phanerozoic time: interpretation using a flux model. Geochim. Cosmochim. Acta 40, 721–730.
Brown, K.A., Williams, W.J., Carmack, E.C., Fiske, G., Francois, R., McLennan, D., Peucker-Ehrenbrink, B., 2018. Geochemistry of small Canadian Arctic rivers with diverse geological and hydrological settings. J. Geophys. Res. Biogeosci (in review).
Buck, W.R., 1991. Modes of continental lithospheric extension. J. Geophys. Res. 96 (B12), 20,161–20,178.
Buhl, D., Neuser, R.D., Richter, D.K., Riedel, D., Roberts, B., Strauss, H., Veizer, J., 1991. Nature and nurture: environmental isotope story of the Rhine River. Naturwissenschaften 78, 337–346.
Burke, W.H., Denison, R.E., Hetherington, E.A., Koepnick, R.B., Nelson, H.F., Otto, J.B., 1982. Variations of seawater $^{87}Sr/^{86}Sr$ through Phaneroizoic time. Geology 10, 516–519.
Butterfield, D.A., Nelson, B.K., Wheat, C.G., Mottl, M.J., Roe, K.K., 2001. Evidence for basaltic Sr in midocean ridge-flank hydrothermal systems and implications for the global oceanic Sr isotope balance. Geochim. Cosmochim. Acta 65, 4141–4153.
Cameron, E.M., Hattori, K., 1997. Strontium and neodymium isotope ratios in the Fraser River, British Columbia: a riverine transect across the Cordilleran orogen. Chem. Geol. 137, 243–253.
Cao, W., Lee, C.-T.A., Lackey, J.S., 2017. Episodic nature of continental arc activity since 750 Ma: a global compilation. Earth Planet. Sci. Lett. 461, 85–95.
Chapman, H., Bickle, M., Thaw, S.H., Thiam, H.N., 2015. Chemical fluxes from time series sampling of the Irrawaddy and Salween Rivers, Myanmar. Chem. Geol. 401, 15–27.
Charette, M.A., Smith, W.H.F., 1999. The volume of the Earth's ocean. Oceanography 23 (2), 112–114.
Chaudhuri, S., Clauer, N., 1986. Fluctuations of isotopic composition of strontium in seawater during the Phanerozoic eon. Chem. Geol. (Isotope Geosci. Sec.) 59, 293–303.
Cogné, J.-P., Humler, E., 2004. Temporal variations of oceanic spreading and crustal production rates during the last 180 My. Earth Planet. Sci. Lett. 227, 427–439.
Cogné, J.-P., Humler, E., 2006. Trends and rhythms in global seafloor generation rate. Geochem. Geophys. Geosyst. 7, Q03011. https://doi.org/10.1020/2005GC001148.
Commission for the Geologic Map of the World, 2000. Geologic Map of the World at 1:25,000,000, 2nd edition. UNESCO.
Coogan, L.A., Dosso, S.E., 2012. An internally consistent, probabilistic, determination of ridge-axis hydrothermal fluxes from basalt-hosted systems. Earth Planet. Sci. Lett. 323–324, 92–101.
Coogan, L.A., Dosso, S.E., 2015. Alteration of ocean crust provides a strong temperature dependent feedback on the geological carbon cycle and is a primary driver of the Sr-isotopic composition of seawater. Earth Planet. Sci. Lett. 415, 38–46. https://doi.org/10.1026/j.epsl.2015.01.027.
Corliss, J.B., Dymond, J., Gordon, L.I., Edmond, J.M., von Herzen, R.P., Ballard, R.D., Green, K., Williams, D., Bainbridge, A., Crane, K., van Andel, T.H., 1979. Submarine thermal springs on the Galápagos Rift. Science 203, 1073–1083.
Dasch, E.J., Biscaye, P.E., 1971. Isotopic composition of strontium in Cretaceous-to-recent pelagic foraminifera. Earth Planet. Sci. Lett. 11, 201–204.
Dasch, E.J., Hedge, C.E., Dymond, J., 1973. Effect of sea water interaction on strontium isotope composition of deep-sea basalts. Earth Planet. Sci. Lett. 19, 177–183.
Davis, A.C., Bickle, M.J., Teagle, D.A.H., 2003. Imbalance in the oceanic strontium budget. Earth Planet. Sci. Lett. 211, 173–187.
de Villiers, S., 1999. Seawater strontium and Sr/Ca variability in the Atlantic and Pacific oceans. Earth Planet. Sci. Lett. 171, 623–634.
de Villiers, S., Compton, J.S., Lavelle, M., 2000. Strontium isotope systematics of the Orange River, Southern Africa. S. Afr. J. Geol. 103 (3–4), 237–248.
DePaolo, D.J., 1981. Neodymium isotopes in the Colorado Front Range and crust-mantle evolution in the Proterozoic. Nature 291, 193–196.
Dhuime, B., Hawkesworth, C.J., Cawood, P.A., Storey, C.D., 2012. A change in the geodynamics of continental growth 3 billion years ago. Science 335, 1334–1336.
Dickinson, W.R., Patchett, P.J., Ferguson, C.A., Suneson, N.H., Gleason, J.D., 2003. Nd isotopes of Atoka Formation (Pennsylvanian) turbidites displaying anomalous east-flowing paleocurrents in the frontal Ouachita belt of Oklahoma: implications for regional sediment dispersal. J. Geol. 111, 733–740.
Donnadieu, Y., Goddéris, Y., Pierrehumbert, R., Dromart, G., Fluteau, F., Jacob, R., 2006. A GEOCLIM simulation of climatic and biogeochemical consequences of Pangea breakup. Geochem. Geophys. Geosyst. 7 (11), Q11019. https://doi.org/10.1020/2005GC001278.
Douglas, T.A., Chamberlain, C.P., Blum, J.D., 2002. Land use and geologic controls on the major elemental and isotopic ($\delta^{15}N$ and $^{87}Sr/^{86}Sr$) geochemistry of the Connecticut River watershed, USA. Chem. Geol. 189, 19–34.
Edmond, J.M., 1992. Himalayan tectonics, weathering processes, and the strontium isotope record in marine limestones. Science 258, 1594–1597.
Edmond, J.M., Palmer, M.R., Measures, C.I., Brown, E.T., Huh, Y., 1996. Fluvial geochemistry of the eastern slope of the northeastern Andes and its foredeep in the drainage of the Orinoco in Colombia and Venezuela. Geochim. Cosmochim. Acta 60, 2949–2976.
Edmond, J.M., Palmer, M.R., Measures, C.I., Grant, B., Stallard, R.F., 1995. The fluvial geochemistry and denudation rate of the Guayana Shield in Venezuela, Colombia and Brazil. Geochim. Cosmochim. Acta 59, 3301–3325.
Elderfield, H., Gieskes, J.M., 1982. Sr isotopes in interstitial waters of marine sediments from Deep Sea Drilling Project cores. Nature 300, 493–497.
Elderfield, H., Schultz, A., 1996. Mid-ocean ridge hydrothermal fluxes and the chemical composition of the ocean. Annu. Rev. Earth Planet. Sci. 24, 191–224.
Ernst, R.E., Youbi, N., 2017. How Large Igneous Provinces affect global climate, sometimes cause mass extinctions, and represent natural markers in the geological record. Palaeogeogr. Palaeoclimatol. Palaeoecol. 478, 30–52.
Farrell, J.W., Clemens, S.C., Gromet, L.P., 1995. Improved chronostratigraphic reference curve of late Neogene seawater $^{87}Sr/^{86}Sr$. Geology 23, 403–406.
Faure, G., Hurley, P.M., Powell, J.L., 1965. The isotopic composition of strontium in surface water from the North Atlantic Ocean. Geochim. Cosmochim. Acta 29, 209–220.
Faure, G., Crocket, J.H, Hurley, P.M., 1967. Some aspects of the geochemistry of strontium and calcium in the Hudson Bay and the Great Lakes. Geochim. Cosmochim. Acta 31, 451–461.
Fiege, K., Miller, C.A., Robinson, L., Figueroa, R., Peucker-Ehrenbrink, B., 2009. Strontium isotopes in Chilean rivers: the flux of unradiogenic continental Sr to seawater. Chem. Geol. 268, 337–343. https://doi.org/10.1016/CHEMGEO4601.
Gaillardet, J., Dupré, B., Louvat, P., Allègre, C.J., 1999. Global silicate weathering and CO_2 consumption rates deduced from the chemistry of large rivers. Chem. Geol. 159, 3–30.
Galy, A., France-Lanord, C., Derry, L.A., 1999. The strontium isotopic budget of Himalayan rivers in Nepal and Bangladesh. Geochim. Cosmochim. Acta 63 (13/14), 1905–1925.
Galy, V., France-Lanord, C., Peucker-Ehrenbrink, B., Huyghe, P., 2010. Sr-Nd-Os evidence for a stable erosion regime in the Himalaya during the past 12 Myr. Earth Planet. Sci. Lett. 290, 474–480.
Garzione, C.N., Patchett, P.J., Ross, G.M., Nelson, J., 1997. Provenance of Paleozoic sedimentary rocks in the Canadian Cordilleran miogeocline: a Nd isotopic study. Can. J. Earth Sci. 34, 1603–1618.
Gast, P.W., 1955. Abundance of ^{87}Sr during geologic time. Bull. Geol. Soc. Am. 66, 1449–1454.
Gastil, G., 1960. The distribution of mineral dates in time and space. Am. J. Sci. 258, 1–35.
Gastner, M.T., Newman, M.E.J., 2004. Diffusion-based method for producing density-equalizing maps. Proc. Natl. Acad. Sci. 101 (20), 7499–7504.
Gibbs, M.T., Bluth, G.J.S., Fawcett, P.J., Kump, L.R., 1999. Global chemical erosion over the last 250 My: variations due to changes in Paleogeography, Paloclimate, and Paleogeology. Am. J. Sci. 299, 611–651.
Gleason, J.D., Patchett, P.J., Dickinson, W.R., Ruiz, J., 1994. Nd isotope link Ouachita turbidites to Appalachian sources. Geology 22, 347–350.
Gleason, J.D., Patchett, P.J., Dickinson, W.R., Ruiz, J., 1995. Nd isotopic constraints on sediment sources of the Ouachita-Marathon fold belt. GSA Bull. 107 (10), 1192–1210.
Godderis, Y., Donnadieu, Y., Le Hir, G., Levebvre, V., Nardin, E., 2014. The role of paleogeography in the Phanerozoic history of atmospheric CO_2 and climate. Earth Sci. Rev. 128, 122–138.
Godsey, S.E., Kirchner, J.W., Clow, D.W., 2009. Concentration-discharge relationships reflect chemostatic characteristics of US catchments. Hydrol. Proced. 23, 1844–1864. https://doi.org/10.1002/hyp.7315.
Goldstein, S.J., Jacobsen, S.B., 1987. The Nd and Sr isotopic systematics of river-water dissolved material: implications for the sources of Nd and Sr in seawater. Chem. Geol. 66, 245–272.
Goldstein, S.L., 1988. Decoupled evolution of Nd and Sr isotopes in the continental crust and the mantle. Nature 336, 733–738.
Gradstein, F., Ogg, J.G., Schmitz, M., Ogg, G. (Eds.), 2012. The Geologic Time Scale. Elsevier, Boston, pp. 1176.
Graham, S.T., Famiglietti, J.S., Maidment, D.R., 1999. Five minute, ½°, and 1° data sets of continental watersheds and river networks for use in regional and global hydrologic and climate system modeling studies. Water Resour. Res. 35, 583–587.
Graham, S.T., Famiglietti, J.S., Maidment, D.R., 2000. Five-minute, ½°, and 1° data sets of continental watersheds and river networks for use in regional and global hydrologic and climate system modeling studies: watershed and drainage network data evaluated at three spatial resolutions with supporting documentation. In: Digital Data on 5 Minute, ½ Degree and 1 Degree Resolution, Geographic (lat/long) Global Grids. NOAA National Geophysical Data Center, Boulder, CO (Nine spatial layers with multiple attributes).
Hagedorn, B., Hasholt, B., 2004. Hydrology, geochemistry and Sr isotopes in solids and solutes of the meltwater from Mittivakkat Gletscher, SE Greenland. Nord. Hydrol. 35, 369–380.
Hamilton, E.I., 1966. The isotopic composition of strontium in Atlantic Ocean water. Earth Planet. Sci. Lett. 1, 435–436.
Hansen, K.W., Wallmann, K., 2003. Cretaceous and Cenozoic evolution of seawater composition, atmospheric O_2 and CO_2: a model perspective. Am. J. Sci. 303, 94–148.
Hartman, J., Moosdorf, N., 2012. The new global lithologic map database GLiM: A representation of rock properties at the Earth surface. Geochem. Geophys. Geosyst. 13

(12). https://doi.org/10.1029/2012GC004370.
Harvey, C.F., 2002. Groundwater flow in the Ganges delta. Science 296, 1563.
Hindshaw, R.S., Rickli, J., Leuthold, J., Wadham, J., Bourdon, B., 2014. Identifying weathering sources and processes in an outlet glacier of the Greenland Ice Sheet using Ca and Sr isotope ratios. Geochim. Cosmochim. Acta 145, 50–71.
Hodell, D.A., Mead, G.A., Mueller, P.A., 1990. Variation in the strontium isotopic composition of seawater (8 Ma to present): Implications for chemical weathering rates and dissolved fluxes to the oceans. Chem. Geol. 80, 291–307.
Hofmann, A.W., 1988. Chemical differentiation of the Earth: the relationship between mantle, continental crust, and oceanic crust. Earth Planet. Sci. Lett. 90, 297–314.
Hooker, P.J., Hamilton, P.J., O'Nions, R.K., 1981. An estimate of the Nd isotopic composition of Iapetus seawater from ca. 490 Ma metalliferous sediments. Earth Planet. Sci. Lett. 56, 180–188.
Huang, K.-F., You, C.-F., Chung, C.-H., Lin, I.-T., 2011. Nonhomogenous seawater Sr isotopic composition in the coastal oceans: a novel tool for tracing water masses and submarine groundwater discharge. Geochem. Geophys. Geosyst. 12 (5), Q05002. https://doi.org/10.1029/2010GC003372.
Huh, Y., Edmond, J.M., 1999. The fluvial geochemistry of the rivers of Eastern Siberia: III. Tributaries of the Lena and Anabar draining the basement terrain of the Siberian Crator and the Trans-Baikal Highlands. Geochim. Cosmochim. Acta 62, 2039–2051.
Huh, Y., Panteleyev, G., Babich, D., Zaitsev, A., Edmond, J.M., 1998. The fluvial geochemistry of the rivers of Eastern Siberia: II. Tributaries of the Lena, Omoloy, Yana, Indigirka, Koluma, and Anadyr draining the collisional/accretionary zone of the Verkhoyansk and Cherskiy ranges. Geochim. Cosmochim. Acta 62 (12), 2053–2075.
Ingram, B.L., Sloan, D., 1992. Strontium isotopic composition of estuarine sediments as paleosalinity-paleoclimate indicator. Science 255, 68–72.
Jayananda, M., Chardon, D., Peucat, J.-J., Tushipokla, Fanning, C.M., 2015. Paleo- to Mesoarchean TTG accretion and continental growth in the western Dharwar craton, Southern India: Constraints from SHRIMP U-Pb zircon geochronology, whole-rock geochemistry and Nd-Sr isotopes. Precambrian Res. 268, 295–322.
Jones, M.T., Jerram, D.A., Svensen, H.H., Grove, C., 2016. The effects of large igneous provinces on the global carbon and sulphur cycles. Palaeogeogr. Palaeoclimatol. Palaeoecol. 441, 4–21.
Jones, M.T., Pearce, C.R., Jeandel, C., Gislason, S.R., Eiriksdottir, E.S., Mavromatis, V., Oelkers, E.H., 2012. Riverine particulate material dissolution as a significant flux of strontium to the oceans. Earth Planet. Sci. Lett. 355-356, 51–59.
Kent, D.V., Muttoni, G., 2008. Equatorial convergence of India and early Cenozoic climate trends. Proc. Natl. Acad. Sci. https://doi.org/10.1073/pnas.0805382105.
Keto, L.S., Jacobsen, S.B., 1988. Nd isotope variations of Phanerozoic paleoceans. Earth Planet. Sci. Lett. 90, 395–410.
Korte, C., Jasper, T., Kozur, H.W., Veizer, J., 2006. $^{87}Sr/^{86}Sr$ record of Permian seawater. Palaeogeogr. Palaeoclimatol. Palaeoecol. 240, 89–107.
Korte, C., Kozur, H.W., Bruckschen, P., Veizer, J., 2003. Strontium isotope evolution of Late Permian and Triassic seawater. Geochim. Cosmochim. Acta 67 (1), 47–62.
Krabbenhöft, A., Eisenhauer, A., Böhm, F., Vollstaedt, H., Fietzke, J., Liebetrau, V., Augustin, N., Peucker-Ehrenbrink, B., Müller, M.N., Horn, C., Hansen, B.T., Nolte, N., Wallmann, K., 2010. Constraining the marine strontium budget with natural strontium isotope fractionation ($^{87}Sr/^{86}Sr^*$, $\delta^{88/86}Sr$) of carbonates, hydrothermal solutions and river waters. Geochim. Cosmochim. Acta 74, 4097–4109.
Krishnaswami, S., Trivedi, J.R., Sarin, M.M., Ramesh, R., Sharma, K.K., 1992. Strontium isotopes and rubidium in the Ganga-Brahmaputra river system: weathering in the Himalaya, fluxes to the Bay of Bengal and contributions to the evolution of oceanic $^{87}Sr/^{86}Sr$. Earth Planet. Sci. Lett. 109, 243–253.
Kump, L.R., 1989. Alternative modeling approaches to the geochemical cycles of carbon, sulfur, and strontium isotopes. Am. J. Sci. 289, 390–410.
Luo, C., Zheng, H., Tada, R., Wu, W., Irino, T., Yang, S., Saito, K., 2014. Tracing Sr isotopic composition in space and time across the Yangtze River basin. Chem. Geol. 388, 59–70.
Martin, J.-M., Meybeck, M., 1979. Elemental mass-balance of material carried by major world rivers. Mar. Chem. 7, 173–206.
Mavromatis, V., Rinder, T., Prokushkin, A.S., Pokrovsky, O.S., Korets, M.A., Chmeleff, J., Oelkers, E.H., 2016. The effect of permafrost, vegetation, and lithology on Mg and Si isotope composition of the Yenisey River and its tributaries at the end of the spring flood. Geochim. Cosmochim. Acta 191, 32–46.
McArthur, J.M., Howard, R.J., Shields, G.A., 2012. Strontium isotope stratigraphy. In: Gradstein, F.M. (Ed.), The Geologic Time Scale 2012. Elsevier, pp. 127–144.
McArthur, J.M., Howarth, R.J., Bailey, T.R., 2001. Strontium isotope stratigraphy: LOWESS version 3: best fit to the marine Sr-isotope curve for 0–509 Ma and accompanying look-up table for deriving numerical age. J. Geol. 109, 155–170.
McLennan, S.M., 2001. Relationship between the trace element composition of sedimentary rocks and upper continental crust. Geochem. Geophys. Geosyst. 2 (2000GC000109).
Mernild, S.H., Liston, G.E., Hiemstra, C.A., Steffen, K., Hanna, E., Christensen, J.N., 2009. Greenland Ice Sheet surface mass-balance modelling and freshwater flux for 2007, and in a 1995–2007 perspective. Hydrol. Process. 23, 2470–2484.
Meybeck, M., 1986. Composition chimique des ruisseaux non pollués de France. Sci. Géol. Bull. 39 (1), 3–77.
Meybeck, M., 1988. How to establish and use world budgets of riverine materials. In: Lerman, A., Meybeck, M. (Eds.), Physical and Chemical Weathering in Geochemical Cycles. NATO ASI Series, vol. 251. pp. 247–272.
Meybeck, M., 2005. Chemical characteristics of rivers. In: Dooge, J.C.I. (Ed.), Fresh Surface Water. Encyclopedia of Life Support Systems, vol. 1 Developed under the auspices of the UNESCO, Eolss Publishers, Paris, France. http://www.eolss.net.
Michard, A., Albarède, F., Michard, G., Minster, J.F., Charlou, J.L., 1983. Rare-earth elements and uranium in high-temperature solutions from East Pacific Rise hydrothermal vent field (13-degrees N). Nature 303, 795–797.
Milliman, J.D., Farnsworth, K.L., 2011. River Discharge to the Coastal Ocean: A Global Synthesis. Cambridge Univ. Press, 978-0-521-87987-3pp. 392.
Milliman, J.D., Syvitski, J.P.M., 1992. Geomorphic tectonic control of sediment discharge to the ocean – the importance of small mountainous rivers. J. Geol. 100, 525–544.
Mokadem, F., Parkinson, I.J., Hathorne, E.C., Anand, P., Allen, J.T., Burton, K.W., 2015. High-precision radiogenic strontium isotope measurements of the modern and glacial ocean: limits on glacial-interglacial variations in continental weathering. Earth Planet. Sci. Lett. 415, 111–120.
Murthy, R.V., Beiser, E., 1968. Strontium isotopes in ocean water and marine sediments. Geochim. Cosmochim. Acta 32, 1121–1126.
Negrel, P., Dupre, B., 1993. Seasonal Fluctuations of Major, Trace Elements Composition and $^{87}Sr/^{86}Sr$ Ratios of the Congo River. Implications for the Hydrological Functioning and Input to the Ocean. Grands Bassins Fluviaux, Paris, pp. 39–50 22–24 Nov. 1993.
Nielsen, S.G., Rehkämper, M., Teagle, D.A.H., Butterfield, D.A., Alt, J.C., Halliday, A.N., 2006. Hydrothermal fluid fluxes calculated from the isotopic mass balance of thallium in the ocean crust. Earth Planet. Sci. Lett. 251, 120–133.
Noh, H., Huh, Y., Qin, J., Ellis, A., 2009. Chemical weathering in the Three Rivers region of Eastern Tibet. Geochim. Cosmochim. Acta 73, 1857–1877.
Palmer, M.R., Edmond, J.M., 1989. The strontium isotope budget of the modern ocean. Earth Planet. Sci. Lett. 92, 11–26.
Palmer, M.R., Edmond, J.M., 1992. Controls over the strontium isotope composition of river water. Geochim. Cosmochim. Acta 56, 2099–2111.
Palmer, M.R., Elderfield, H., 1985. Sr isotope composition of sea water over the past 75 Myr. Nature 314, 526–528.
Patchett, J.P., Ross, G.M., Gleason, J.D., 1999a. Continental drainage in North America during the Phanerozoic from Nd isotopes. Science 283, 671–673.
Patchett, P.J., Embry, A.F., Ross, G.M., Beauchamp, B., Harrison, J.C., Mayr, U., Isachsen, C.E., Rosenberg, E.J., Spence, G.O., 2004. Sedimentary cover of the Canadian Shield through Mesozoic time reflected by Nd isotopic and geochemical results for the Sverdrup Basin, Arctic Canada. J. Geol. 112, 39–57.
Patchett, P.J., Gehrels, G.E., 1998. Continental influence on Canadian Cordilleran terranes from Nd isotopic study, and significance for crustal growth processes. J. Geol. 106, 269–280.
Patchett, P.J., Roth, M.A., Canale, B.S., de Freitas, T.A., Harrison, J.C., Embry, A.F., Ross, G.M., 1999b. Nd isotopes, geochemistry, and constraints on sources of sediments in the Franklinian mobile belt, Arctic Canada. Geol. Soc. Am. Bull. 111 (4), 578–589.
Pavellek, F., Frauenstein, F., Veizer, J., 2002. Hydrochemistry and isotope geochemistry of the upper Danube River. Geochim. Cosmochim. Acta 21, 3839–3854.
Pearce, C.R., Parkinson, I.J., Gaillardet, J., Charlier, B.L.A., Mokadem, F., Burton, K.W., 2015. Reassessing the stable ($\delta^{88/86}Sr$) and radiogenic ($^{87}Sr/^{86}Sr$) strontium isotopic composition of marine inputs. Geochim. Cosmochim. Acta 157, 125–146.
Peterman, Z.E., Hedge, C.E., Tourtelot, H.A., 1970. Isotopic composition of Sr in seawater throughout Phanerozoic time. Geochim. Cosmochim. Acta 34, 105–120.
Peucker-Ehrenbrink, B., 2009. Land2Sea database of river drainage basin sizes, annual water discharges and suspended sediment fluxes. Geochem. Geophys. Geosyst. 10 (6), Q06014. https://doi.org/10.1029/2008GC002356.
Peucker-Ehrenbrink, B., 2018. Land2Sea Database, Version 2.0. Pangaea. https://doi.org/10.1594/PANGAEA.892680.
Peucker-Ehrenbrink, B., Miller, M.W., 2002. Quantitative bedrock geology of the conterminous United States of America. Geochem. Geophys. Geosyst. 3 (10), 8000. https://doi.org/10.1029/2002GC000366.
Peucker-Ehrenbrink, B., Miller, M.W., 2003. Quantitative bedrock geology of Alaska and Canada. Geochem. Geophys. Geosyst. 4 (4), 8005. https://doi.org/10.1029/2002GC000449.
Peucker-Ehrenbrink, B., Miller, M.W., 2004. Quantitative bedrock geology of East and Southeast Asia (Brunei, Cambodia, eastern and southeastern China, East Timor, Indonesia, Japan, Laos, Malaysia, Myanmar, North Korea, Papua New Guinea, Philippines, far eastern Russia, Singapore, South Korea, Taiwan, Thailand, Vietnam). Geochem. Geophys. Geosyst. 5 (1), Q01B06. https://doi.org/10.1029/2003GC000619.
Peucker-Ehrenbrink, B., Miller, M.W., 2007a. Quantitative bedrock geology of Brazil. Geochem. Geophys. Geosyst. 8 (5), Q05014. https://doi.org/10.1029/2006GC001505.
Peucker-Ehrenbrink, B., Miller, M.W., 2007b. Quantitative bedrock geology of the continents and large-scale drainage regions. Geochem. Geophys. Geosyst. 8 (5), Q06009. https://doi.org/10.1029/2006GC001544.
Peucker-Ehrenbrink, B., Miller, M.W., Arsouze, T., Jeandel, C., 2010. Continental bedrock and riverine fluxes of strontium and neodymium isotopes to the oceans. Geochem. Geophys. Geosyst. 11 (3), Q03016. https://doi.org/10.1029/2009GC002869.
Peucker-Ehrenbrink, B., Ravizza, G., 2001. The marine Os isotope record. Terra Nova 12 (5), 205–219.
Peucker-Ehrenbrink, B., Ravizza, G., 2012. Chapter 8: osmium isotope stratigraphy. In: Gradstein, F., Ogg, J., Schmitz, M., Ogg, G. (Eds.), The Geologic Time Scale 2012. Elsevier, Boston, pp. 145–166. https://doi.org/10.1016/B978-0-444-59425-9.00008-1.
Plank, T., Langmuir, C.H., 1998. The chemical composition of subducting sediment and its consequences for the crust and mantle. Chem. Geol. 145, 325–394.
Plumb, K.A., 1991. New Precambrian time scale. Episodes 14, 139–140.
Pouilly, M., Point, D., Sondag, F., Henry, M., Santos, R.V., 2014. Geographical origin of Amazonian freswater fishes fingerprinted by $^{87}Sr/^{86}Sr$ ratios on fish otoliths and scales. Environ. Sci. Technol. 48, 8980–8987.
Rahaman, W., Singh, S.K., Sinha, R., Tandon, S.K., 2011. Sr, C and O isotopes in carbonate nodules from the Ganga Plain: evidence for recent abrupt rise in dissolved $^{87}Sr/^{86}Sr$ ratio of the Ganga. Chem. Geol. 285, 184–193.
Rai, S.K., Singh, S.K., 2007. Temporal variation in Sr and $^{87}Sr/^{86}Sr$ of the Brahmaputra:

Implications for annual fluxes and tracking flash floods through chemical and isotope composition. Geochem. Geophys. Geosyst. 8 (8), Q08008. https://doi.org/10.1029/2007GC001610.
Raymo, M.E., Ruddiman, W.F., Froehlich, P.N., 1988. Influence of late Cenozoic mountain building on ocean geochemical cycles. Geology 16, 649–653.
Reed, B.C., 1992. Linear least-squares fit with errors in both coordinates. II: comments on parameter variances. Am. J. Phys. 60, 59–62.
Reed, B.C., 2010. A spreadsheet for linear least-squares fitting with errors in both coordinates including covariance. Phys. Educ. 45 (1), 93–96.
Reeder, S.W., Hitchon, B., Levinson, A.A., 1972. Hydrogeochemistry of the surface waters of the Mackenzie River drainage basin, Canada – I. Factors controlling inorganic composition. Geochim. Cosmochim. Acta 36, 825–865.
Richter, F.M., Rowley, D.B., DePaolo, D.J., 1992. Sr isotope evolution of seawater: the role of tectonics. Earth Planet. Sci. Lett. 109, 11–23.
Rink, H., 1863. On the discharge of water from the interior of Greenland, through springs underneath the ice. Proc. R. Geogr. Soc. Lond. 7 (2), 76–78.
Ronov, A.B., 1989. Atlas of Lithological-Paleogeographical Maps of the World. Mesozoic and Cenozoic of Continents and Oceans. Nauk, Leningrad, pp. 79.
Ronov, A.B., 1993. In: Yaroshevskii, A.A. (Ed.), Stratisfera – Iii Osadochnaya Obolochka Zemli (Kolichestvennoe Issledavanie). Nauk, Moskva, pp. 144 (in Russian).
Ross, G.M., Patchett, P.J., Hamilton, M., Heaman, L., DeCelles, P.G., Rosenberg, E., Giovanni, M.K., 2005. Evolution of the Cordilleran orogen (southwestern Alberta, Canada) inferred from detrital mineral geochronology, geochemistry, and Nd isotopes in the foreland basin. GSA Bull. 117 (5/6), 747–763. https://doi.org/10.1130/B25564.1.
Rotenberg, E., Davis, D.W., Amelin, Y., Gosh, S., Bergquist, B.A., 2012. Determination of the decay-constant of ^{87}Rb by laboratory accumulation of ^{87}Sr. Geochim. Cosmochim. Acta 85, 41–57.
Rowley, D.B., 2002. Rate of plate creation and destruction: 180 Ma to present. Geol. Soc. Am. Bull. 114, 927–933.
Santos, R.V., Sondag, F., Cochonneau, G., Lagane, C., Brunet, P., Hattingh, K., Chaves, J.G.S., 2015. Source area and seasonal ^{87}Sr/^{86}Sr variations in rivers of the Amazon basin. Hydrol. Proced. 29, 187–197.
Schildgen, T.F., Cosentino, D., Frijia, G., Castorina, F., Dudas, Ö., Iadanza, A., Sampalmieri, G., Cipollari, P., Caruso, A., Bowring, S.A., Strecker, M.R., 2014. Sea level and climate forcing of the Sr isotope composition of late Miocene Mediterranean marine basins. Geochem. Geophys. Geosyst. 15, 2964–2983. https://doi.org/10.1002/2014GC005332.
Scribner, C.A., Martin, E.E., Martin, J.B., Deuerling, K.M., Collazo, D.F., Marshall, A.T., 2015. Exposure age and climate controls on weathering in deglaciated watersheds of western Greenland. Geochim. Cosmochim. Acta 170, 157–172.
Semhi, K., Clauer, N., Probst, J.L., 2000. Strontium isotope compositions of river waters as records of lithology-dependent mass transfers: the Garonne river and its tributaries (SW France). Chem. Geol. 168, 173–193.
Seyler, P.T., Boaventura, G.R., 2003. Distribution and partition of trace metals in the Amazon basin. Hydrol. Proced. 17, 1345–1361. https://doi.org/10.1002/hyp.1288.
Shields, G., Veizer, J., 2002. Precambrian marine carbonate isotope database: version 1.1. Geochem. Geophys. Geosyst. 3 (6). https://doi.org/10.1029/2001GC000266.
Spooner, E.T.C., 1976. The strontium isotopic composition of seawater, and seawater-oceanic crust interaction. Earth Planet. Sci. Lett. 31, 167–174.
Stallard, R.F., Edmond, J.M., 1983. Geochemistry of the Amazon 2. The influence of geology and weathering environment on the dissolved load. J. Geophys. Res. 88, 9671–9688.
Steiger, R.H., Jäger, E., 1977. Subcommission on geochronology: convention on the use of decay constants in geo- and cosmochronology. Earth Planet. Sci. Lett. 36, 359–362.
Tachikawa, K., Athias, V., Jeandel, C., 2003. Neodymium budget in the modern ocean and paleo-oceanographic implications. J. Geophys. Res. 108 (C8). https://doi.org/10.1029/1999JC000285.
Tardy, Y., N'Kounkou, R., Probst, J.-L., 1989. The global water cycle and continental erosion during Phaneroizoic time (570 my). Am. J. Sci. 289, 455–483.
Thorsvik, T.H., Smethurst, M.A., Burke, K., Steinberger, B., 2008. Long term stability in deep mantle structure: evidence from the ca. 300 Ma Skagerrak-Centered Large Igneous Province (the SCLIP). Earth Planet. Sci. Lett. 267, 444–452.
Trezzi, G., Garcia-Orellana, J., Rodellas, V., Masque, P., Garcia-Solsona, E., Andersson, P.S., 2016. Assessing the role of submarine groundwater discharge as a source of Sr to the Mediterranean Sea. Geochim. Cosmochim. Acta, GCA10057. https://doi.org/10.1016/j.gca.2016.12.005.
Tripathy, G.R., Goswami, V., Singh, S.K., Chakrapani, G.J., 2010. Temporal variations in Sr and ^{87}Sr/^{86}Sr of the Ganga headwaters: estimates of dissolved Sr flux to the mainstream. Hydrol. Process. 24 (9), 159–1171.
van der Flierdt, T., Griffith, A.M., Lambelet, M., Little, S.H., Stichel, T., Wilson, D.J., 2016. Neodymium in the oceans: a global database, a regional comparison and implications for palaeoceanographic research. Phil. Trans. R. Soc. A 374, 20150293. https://doi.org/10.1098/rsta.2015.0293.
Van Der Meer, D.W., Zeebe, R.E., van Hinsbergen, D.J.J., Sluijs, A., Spakman, W., Torsvik, T.H., 2014. Plate tectonic controls on atmospheric CO_2 level since the Triassic. Proc. Natl. Acad. Sci. 111, 4380–4385.
Van Eysinga, F.W.B., 1975. Geological Timetable, 3rd ed. Elsevier, Amsterdam (compiler).
Van Kranendonk, M.J., 2012. A chronostratigraphic division of the Precambrian – possibilities and challenges. In: Gradstein, F., Ogg, J., Schmitz, M., Ogg, G. (Eds.), The Geologic Time Scale 2012, pp. 299–392 Chapter 16. (with contributions from Altermann, W., Beard, B.L., Hoffman, P.F., Johnson, C.M., Kasting, J.F., Melezhik, V.A., Nutman, A.P., Papineau, D., Pirajno, F.).
Vance, D., Teagle, D.A.H., Foster, G.L., 2009. Variable Quaternary chemical weathering fluxes and imbalances in marine geochemical budgets. Nature 458, 493–496.
Veizer, J., 1989. Strontium isotopes in seawater through time. Annu. Rev. Earth Planet. Sci. 17, 141–167.
Veizer, J., Ala, D., Azmy, K., Bruckschen, P., Buhl, D., Bruhn, F., Carden, G.A.F., Diener, A., Ebneth, S., Godderis, Y., Jasper, T., Korte, C., Pawellek, F., Podlaha, O.G., Strauss, H., 1999. ^{87}Sr/^{86}Sr, δ^{13}C and δ^{18}O evolution of Phanerozoic seawater. Chem. Geol. 161, 59–88.
Veizer, J., Compston, W., 1974. ^{87}Sr/^{86}Sr composition of seawater during the Phanerozoic. Geochim. Cosmochim. Acta 38, 1461–1484.
Voss, B.M., Peucker-Ehrenbrink, B., Eglinton, T.I., Fiske, G., Wang, Z.A., Hoering, K.A., Montluçon, D.B., LeCroy, C., Pal, S., Marsh, S., Gillies, S.L., Janmaat, A., Bennett, M., Downey, B., Fanslau, J., Fraser, H., Macklam-Harron, G., Martinec, M., Wiebe, B., 2014. Tracing river chemistry in space and time: Dissolved inorganic constituents of the Fraser River, Canada. Geochim. Cosmochim. Acta 124, 283–308. https://doi.org/10.1016/j.gca.2013.09.006.
Wadleigh, M.A., Veizer, J., Books, C., 1985. Strontium and its isotopes in Canadian rivers: fluxes and global implications. Geochim. Cosmochim. Acta 49, 1727–1736.
Wickman, F.E., 1948. Isotope ratios: a clue to the age of certain marine sediments. J. Geol. 56, 61–66.
Wilkinson, B.H., McElroy, B.J., Kesler, S.E., Peters, S.E., Rothman, E.D., 2009. Global geologic maps are tectonic speedometers – rates of rock cycling from area-age frequencies. Geol. Soc. Am. Bull. 212, 760–779.
Willmes, M., Glessner, J.J.G., Carleton, S.A., Gerrity, P.C., Hobbs, J.A., 2016. ^{87}Sr/^{86}Sr isotope ratio analysis by laser ablation MC-ICP-MS in scales, spines, and fin rays as a nonlethal alternative to otoliths for reconstructing fish life history. Can. J. Fish. Aquat. Sci. 73, 1852–1860. https://doi.org/10.1139/cjfas-2016-0103.
Wilson, J.T., 1949. The origin of continents and Precambrian history. Roy. Soc. Can. Trans. 43 (3), 157–182.
Wold, C.N., Hay, W.W., 1990. Estimating ancient sediment fluxes. Am. J. Sci. 290, 1069–1089.